JCI The Journal of Clinical Investigation

Stromal integrin α11 regulates PDGFR-β signaling and promotes breast cancer progression

Irina Primac, … , Donald Gullberg, Agnès Noel

J Clin Invest. 2019. https://doi.org/10.1172/JCI125890.

Research In-Press Preview Cell biology Oncology

Graphical abstract

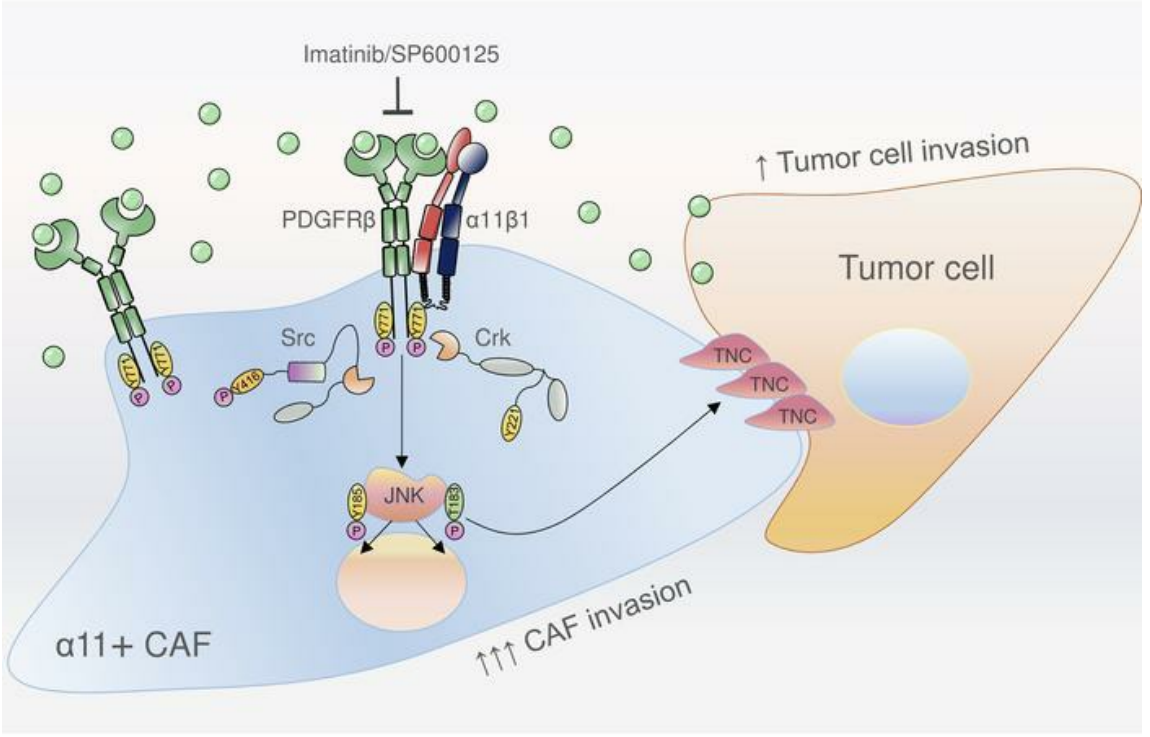

Stromal integrin α11 regulates PDGFR-β signalling and promotes breast cancer progression

Irina Primac[1], Erik Maquoi[1], Silvia Blacher[1], Ritva Heljasvaara[2,3], Jan Van Deun[4], Hilde YH Smeland[3], Annalisa Canale[1], Thomas Louis[1], Linda Stuhr[3], Nor Eddine Sounni[1], Didier Cataldo[1], Taina Pihlajaniemi[2], Christel Pequeux[1], Olivier De Wever[4], Donald Gullberg[3] and Agnès Noel[1#]

[1] Laboratory of Tumor and Development Biology, GIGA-Cancer, University of Liege (ULiège), Liege, Belgium
[2] Oulu Centre for Cell-Extracellular Matrix Research and Biocenter Oulu, Faculty of Biochemistry and Molecular Medicine, University of Oulu, Finland
[3] Department of Biomedicine and Centre for Cancer Biomarkers (CCBIO), Norwegian Centre of Excellence, University of Bergen, Bergen, Norway
[4] Laboratory of Experimental Cancer Research, Department of Human Structure and Repair, Ghent University, Ghent, Belgium

Condensed title: α11 integrin regulates PDGFRβ signalling in CAFs

[#]**Corresponding author:**
Agnès Noel
GIGA-Cancer - Laboratoire de Biologie des Tumeurs et du Développement
Avenue Hippocrate, 13
Tour de Pathologie B23/+4
Sart-Tilman, 4000 Liège
Belgium
Tel: 04/366.25.68
Fax: 04/366.29.36
Email: agnes.noel@uliege.be

ABSTRACT

Cancer-associated fibroblasts (CAFs) are key actors in modulating the progression of many solid tumors such as breast cancer (BC). Herein, we identify an integrin α11/PDGFRβ+ CAF subset displaying tumor-promoting features in BC. In the preclinical MMTV-PyMT mouse model, integrin α11-deficiency led to a drastic reduction of tumor progression and metastasis. A clear association between integrin α11 and PDGFRβ was found at both transcriptional and histological levels in BC specimens. High stromal integrin α11/PDGFRβ expression was associated with high grades and poorer clinical outcome in human BC patients. Functional assays using five CAF subpopulations (one murine, four human) revealed that integrin α11 promotes CAF invasion and CAF-induced tumor cell invasion upon PDGF-BB stimulation. Mechanistically, integrin α11 pro-invasive activity relies on its ability to interact with PDGFRβ in a ligand-dependent manner and to promote its downstream JNK activation, leading to the production of tenascin C, a pro-invasive matricellular protein. Pharmacological inhibition of PDGFRβ and JNK impaired tumor cell invasion induced by integrin α11-positive CAFs. Collectively, our study uncovers an integrin α11-positive subset of pro-tumoral CAFs that exploits PDGFRβ/JNK signalling axis to promote tumor invasiveness in BC.

GRAPHICAL ABSTRACT

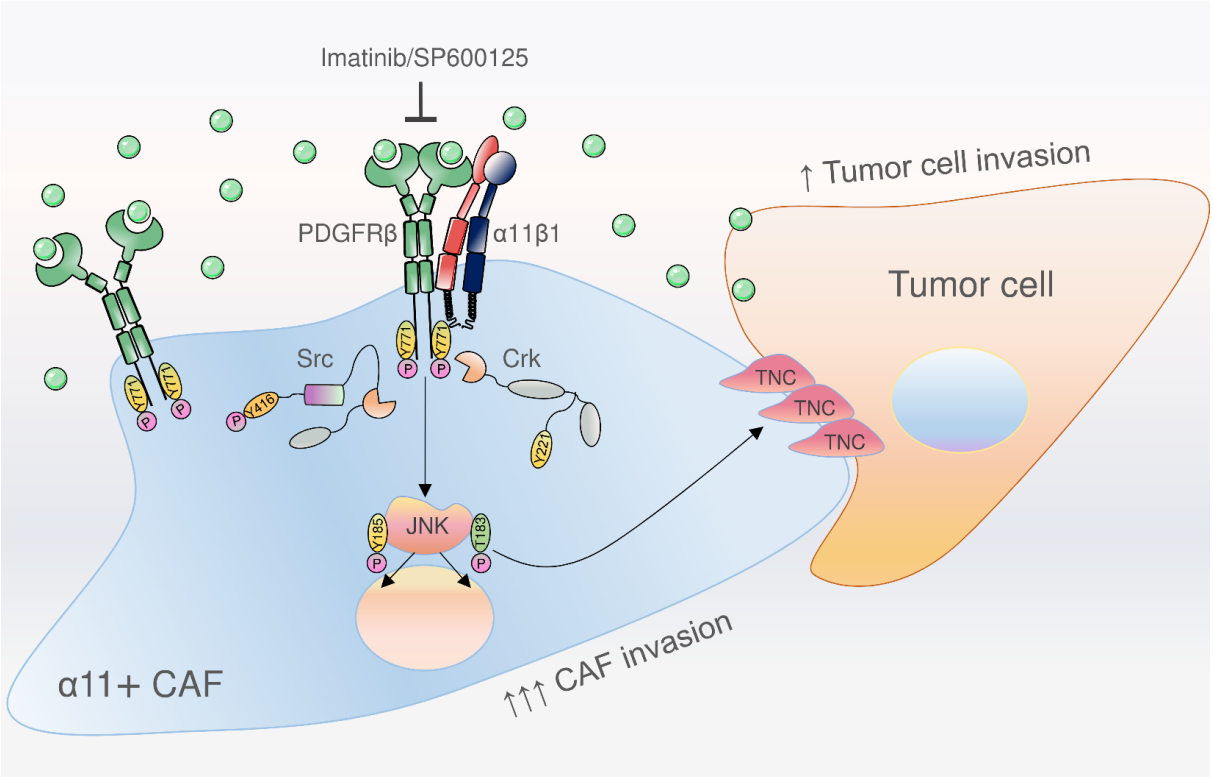

INTRODUCTION

Breast cancer (BC) is the most common type of cancer and the second leading cause of cancer-related death in women worldwide. Despite increasing knowledge of BC biology and huge progress in early detection, approximately 30% of patients with early-stage BC experience disease recurrence (1). Development and progression of cancer are intimately regulated by an evolving crosstalk between tumor cells and surrounding stromal cells, which are composed of immune/inflammatory cells, endothelial cells, pericytes and cancer-associated fibroblasts (CAFs) (2).

CAFs comprise a very heterogeneous cell population derived from different cellular sources including resident fibroblasts, bone marrow–derived progenitor cells, adult mesenchymal stem cells, epithelial and endothelial cells, pericytes and pre-adipocytes (3-5). Due to the heterogeneous feature of CAFs, there is no single molecular marker defining those fibroblastic cells. The most common marker, alpha smooth muscle actin (αSMA) is used to define the activated state of fibroblasts, also known as “myofibroblasts”, although recent data from fibrosis models suggest that αSMA is an inconsistent marker of activated fibroblasts (6). Other molecules such as fibroblast-activating protein (FAP), fibroblast-specific protein (FSP1), platelet derived growth factor receptors (PDGFRs) and neural/glial antigen 2 (NG2) are also considered as CAF markers, but they are neither exclusively specific for this cell type, nor expressed by all CAFs (7, 8). CAFs have been shown to contribute to most of the hallmarks of cancer (9). Classically, pro-tumorigenic effects leading to increased tumor growth, invasion and metastasis are assigned to CAFs. Those direct or indirect effects are related, at least, to their capacity to produce growth factors (5), to promote angiogenesis (10), inflammation (11) and immune response (12), to regulate metabolic reprogramming (13) and to contribute to the remodelling and mechano-transduction of

the extracellular matrix (ECM) (14). Although there is mounting evidence that CAFs are good targets for new anti-cancer therapies (5, 15), recent studies reported tumor-inhibitory effects of CAFs on tumor progression. Indeed, the genetic depletion of αSMA+ CAFs in preclinical models of pancreatic cancer led, surprisingly, to increased tumor growth rather than to an expected reduced cancer progression (16, 17). Altogether, these data highlight CAF heterogeneity, not only in terms of cellular sources and biomarkers, but also in their capacity to promote or inhibit tumor progression. Identifying molecular determinants of functionally distinct CAF subsets is therefore critical to elucidate the contrasting biological actions of these stromal cells during cancer progression.

Tumor and stroma-derived PDGFs (PDGF-AA, PDGF-BB, PDGF-AB, PDGF-CC and PDGF-DD) signal by binding to their tyrosine kinase receptors (PDGFRα and β) and play a key role in the recruitment and phenotypic features of CAFs that infiltrate BCs (18-20). PDGFs initiate the desmoplastic reaction, stimulate angiogenesis, and promote tumor growth and metastatic dissemination (21). PDGF signalling in CAFs has been shown to act as a determinant of the molecular subtype in BC (18). Previous studies have also reported that PDGFRβ expression in fibroblasts of BC patients is associated with aggressiveness, poor prognosis and altered therapeutic response (22, 23). PDGFRβ signalling is not only regulated by growth factors but also by a functional interplay with integrins (24-26). Recently, integrin α11 (ITGA11), a collagen-binding mesenchymal integrin emerged as a novel CAF marker (27). The expression of this integrin is correlated with myofibroblast differentiation, matrix reorganization and collagen deposition (28-30). While integrin α11 function in wound healing has been well described (31), only a very limited number of reports have assessed its role in cancer. In lung cancer, stromal integrin α11 has been reported to increase the

tumorigenicity of cancer cells by regulating IGF-2 production (32) and matrix stiffness (33). The contribution of integrin α11 in BC progression and its crosstalk with the surrounding tyrosine kinase receptors has not been yet documented. Prompted by findings of prominent integrin α11 expression in human BCs, we set out to identify the subset of CAFs expressing integrin α11, to investigate its contribution in BC growth and invasion *in vitro* and *in vivo*, and to molecularly define its role in CAF functions.

RESULTS

Genetic *Itga11* ablation in mice delays tumor growth and drastically reduces metastasis

We used the transgenic polyoma middle T oncogene (PyMT)-induced mouse model (FVB/N genetic background) that accurately reproduces the stepwise progression of human BC with high metastatic dissemination to lungs (34). This model was also chosen for its high content of desmoplasia and infiltrating stromal cells, particularly fibroblasts at all stages of tumor progression. We first assessed integrin α11 expression, both at mRNA and protein levels, at different time points of PyMT primary tumor development. A progressive increase of α11 expression was evidenced from hyperplastic nodules (5 weeks) to carcinoma tumors (10-14 weeks) (Figure 1, A and B). *Itga11*-deficient mice (*Itga11*-/- FVB/N genetic background) were crossed with PyMT mice, resulting in two groups of female mice, hemizygous for PyMT transgene: PyMT *Itga11*+/+ (WT) and PyMT *Itga11*-/- (KO). Phenotypically, *Itga11*-deficient mice show a dwarfism, increased mortality and defective incisors (35) that were maintained in the generated PyMT *Itga11* KO mice. *Itga11* genetic ablation led to a significant delay in the appearance of palpable tumors (Figure 1C) and reduction of tumor growth (Figure 1, D and E). The average time for tumor appearance in 50% of mice was 8 weeks in WT mice and 12 weeks in KO mice (Figure 1C). Tumor volume at sacrifice (week 14) was > 5-fold reduced (Figure 1, D-F) in KO PyMT mice compared to WT PyMT mice. A tumor growth delay of about 3 weeks was observed between the two genotypes when a group of KO PyMT mice was left for longer than 14 weeks ("KO late"), until tumors reached a volume of 1000 mm^3 as observed in WT mice at 14 weeks (Figure 1G). This group was monitored until week 18. WT PyMT tumors were characterized by large and dense tumor lobules with high collagen content (Figure 1H

and Supplemental Figure 1, A and B). In contrast, KO PyMT tumors were composed of small lobules intermingled with adipose tissue and less collagen deposition (Figure 1H and Supplemental Figure 1 A and B). Strikingly, *Itga11*-deficiency dramatically reduced metastasis formation (Figure 2, A-C). At week 14, a twice lower incidence of pulmonary metastases was seen in KO mice (40% of KO mice *vs* 100% of WT mice) (Figure 2B). Importantly, such defect in lung metastasis incidence was still pronounced at later time points ("KO late" group: > weeks 14) when tumors reached a volume of 1000 mm^3 (Figure 2, B and C). Of note, only "KO" and "KO late" mice with metastasis (5/12 and 4/8 mice, respectively) were taken into account for metastatic index determination (Figure 2C).

Integrin α11 defines a subset of PDGFRβ+ CAFs

Immunohistochemical (IHC) stainings were conducted on primary PyMT tumors at different stages (Figure 3A). Anti-α11 antibody specificity was assessed by using *Itga11*-deficient PyMT tumors (Figure 3A). Integrin α11 positivity was easily detected at week 10 and intense at week 14 (Figure 3A). As expected, integrin α11 staining was mostly restricted to the stromal compartment, confirmed also by the absence of association with pan-cytokeratin (Supplemental Figure 1C). Remarkably, integrin α11 strongly colocalized with PDGFRβ and poorly associated to other stromal markers such as αSMA, PDGFRα, NG2 (Figure 3A), FAP, or FSP1 (Supplemental Figure 1D). Of note, PDGFRβ staining was concomitantly detected in early tumors with NG2 (weeks 5 and 7), a pericyte marker (Figure 3A). A computerized quantification revealed that 60% of total α11+ cells were positive for PDGFRβ, while a low proportion of these cells were also positive for another marker: PDGFRα (< 9%), αSMA (< 9%), FAP (< 23%), FSP1 (< 6%) or NG2 (< 12%) (Figure 3A, Supplemental Figure 1D). Thus, α11

integrin is mainly expressed by PDGFRβ+ CAFs. Accordingly, higher levels of PDGFRβ mRNAs (Figure 3B) and proteins (Figure 3C) were detected in PyMT tumors compared to hyperplastic tissues. In sharp contrast to its counterpart isoform, PDGFRα expression was poorly modulated during PyMT tumor progression and not related to integrin α11 expression (Supplemental Figure 1, E and F).

To determine whether tumor resident CAFs or other host integrin α11+ cells are responsible of the observed phenotype, *Itga11* WT PyMT tumors were engrafted into *Itga11* WT and KO receiver mice (Supplemental Figure 2A). Similar tumor growth and mass (Supplemental Figure 2, A-C) were observed in both receiver mice. Histologically, transplanted tumors showed undistinguishable large and invasive tumor lobules (Supplemental Figure 2D) with strong stromal integrin α11/PDGFRβ expression (Supplemental Figure 2E). This demonstrates that integrin α11+ resident CAFs are sufficient to promote tumor progression in an environment proficient or deficient in *Itga11*.

ITGA11 expression is increased in human breast cancers

To determine whether integrin α11 expression is altered in human BC, a meta-analysis of publicly available gene expression data using the Oncomine database was performed. We compared *ITGA11* expression in 2415 BC *vs* 261 normal adjacent BC samples from eight datasets. *ITGA11* was found overexpressed in BC samples (gene median rank: 2476.0, P = 1.92e-10) in seven out of the eight datasets included in the meta-analysis (Figure 4A and Supplemental Table 1). Further analyses showed increased *ITGA11* mRNA levels in BC samples including invasive ductal BC (Figure 4, B-C and F-H), invasive lobular BC (Figure 4C), invasive BC (Figure 4, C and E), ductal BC *in situ* (Figure 4H), tubular BC (Figure 4B) and mixed lobular and ductal BC (Figure

4C) as compared with the corresponding normal breast tissues ($P < 0.05$). The high variance of *ITGA11* expression observed in some tumor groups might result from interindividual and intratumoral heterogeneities.

Oncomine analysis of additional cancer datasets confirmed *ITGA11* overexpression in several types of cancer relative to matched normal tissue including lung, pancreas, colorectal and gastric cancers (Supplemental Figure 3).

In addition, Kaplan-Meier analysis on BC patients stratified by *ITGA11* mRNA levels showed that high *ITGA11* mRNA level (probe 23335_at) is correlated with lower overall (Figure 4I) and distant metastasis-free (Figure 4J) survivals than patients with low *ITGA11* mRNA levels. Similar results were obtained with two other *ITGA11* probes (222899_at and 1554819_a_at). Collectively, these *in silico* data suggest that increased integrin *ITGA11* mRNA levels observed in human BC associate with a worse prognosis.

ITGA11 expression correlates with a stromal gene signature in human BC

Given the stromal integrin α11 expression, we used Gene Expression Omnibus (GEO) microarray datasets to analyze the global gene expression in microdissected human BC specimens: GSE14548; GSE33692; GSE41228 (36) and GSE68744 (Figure 5, A-D). Elevated *ITGA11* expression was found in the stromal compartment as compared to the epithelia of both ductal carcinoma *in situ* (DCIS) and intraductal (IDC)/invasive breast (IBC) carcinomas (Figure 5, A-D). Furthermore, microarray datasets (GSE8977; GSE9014 and GSE14548) comparing stroma microdissected from normal breast and BC samples unveiled a significantly increased *ITGA11* expression in cancerous stroma (Supplemental Figure 4, A-C).

Next, we searched for genes whose expression profile was best correlated (Pearson's

correlation coefficient > 0.5) to *ITGA11* mRNA levels in BC samples. A data mining was conducted in three BC cohorts by using cBioPortal (TCGA breast and Metabric) and bc-GenExMiner genomic tool (36 datasets including 5861 BC patients). For each cohorts (TCGA, Metabric and GenExMiner), genes with Pearson's correlation coefficients > 0.5 were selected and intersected (Figure 5E and Supplemental Table 2) to produce a single list of co-expressed genes (n = 51) defined as the *ITGA11*-associated gene signature. Pathway enrichment analysis using the Reactome knowledgebase (37) revealed that pathways significantly (FDR *Q*-value < 0.05) enriched in *ITGA11*-associated gene signature included at least: *extracellular matrix organization, collagen degradation, integrin cell surface interactions* and *signalling by PDGF* (Figure 5F and Supplemental Table 3).

To further characterize the cell subset expressing *ITGA11* in human BC, we correlated its mRNA expression levels with twelve genes representative of different tumor-associated cell populations. In bc-GenExMiner analysis, *ITGA11* mRNA levels poorly correlated with epithelial (E-cadherin/*CDH1*: Pearson's *r* = 0.01), pericyte (chondroitin sulfate proteoglycan NG2/*CSPG4*: *r* = 0.16) and endothelial (*PECAM1*: *r* = 0.04) markers (Figure 5G and Supplemental Figure 4D). In contrast, stronger correlations were observed with several markers of activated fibroblasts including αSMA (*ACTA2*: *r* = 0.41), PDGFRβ (*PDGFRB*: *r* = 0.47), *FAP* (*r* = 0.58), lysyl oxidase (*LOX*: *r* = 0.61), fibrillar collagens (*COL1A1*: *r* = 0.53; *COL3A1*: *r* = 0.45; *COL5A1*: *r* = 0.63) and collagen type X (*COL10A1*: *r* = 0.69). In line with the *in vivo* data, *ITGA11* correlated with *PDGFRB*, but not with *PDGFRA* (*r* = 0.28). Similar results were confirmed in TCGA breast and Metabric cohorts. In addition, TCSBN database (38) was used to analyse the integrative co-expression landscape of integrin α11 with query genes (*CDH1, ACTA2, CSPG4, PDGFRA and PDGFRB*) in normal and tumoral breast

tissues (Supplemental Figure 5). Again, a high *ITGA11* co-expression with stromal markers was found in BC tissues compared to the normal ones. Among the neighbour genes of the *ITGA11* cluster, we found many matrix-related proteins: collagens (*COL3A1, COL4A2, COL6A3, COL10A1, COL11A1* and *COL12A1*), fibronectin (*FN1*), thrombospondin 2 (*THBS2*), lumican (*LUM*), laminin A4 (*LAMA4*), entactin (*NID1*), as well as functional proteins such as *NOX4, PDGFRB* and *LRP1* (Supplemental Figure 5).

Integrin α11/PDGFRβ density associates with a poor outcome in human BC

We next performed double immunostaining of α11 integrin and PDGFRβ in human BC samples and the associated normal tissues of DCIS and IDC (n = 68 of different breast cancer subtypes) (Figure 6A). Densities of integrin α11 or PDGFRβ were 2-3 fold higher in IDC tumors when compared to DCIS (Figure 6, B-D). The increase in integrin α11 and PDGFRβ colocalisation (% of positive cells/tumor area) was more pronounced in IDC versus DCIS (5-fold increase). This was particularly evident in more aggressive BC molecular subtypes (HER2 and TNBC). In line with the mouse study, > 70% of α11+ CAFs were positive for PDGFRβ and > 60% of PDGFRβ+ CAFs were positive for α11 in IDC tumors (Figure 6, E and F). This further supports the concept that integrin α11 is mainly expressed by a subpopulation of PDGFRβ+ CAFs in human BC. Next, we analyzed the association between this α11/PDGFRβ+ CAF subset and patient outcome. A positive correlation between the double α11/PDGFRβ positivity and high proliferation rate (% ki67) was detected (Figure 6G). Furthermore, higher α11/PDGFRβ stromal density was associated to high tumor grade, metastasis and patient mortality (Figure 6, J-H). The analysis of the spatial distribution of α11, PDGFRβ and double positive cells (Figure 6K) revealed that α11/PDGFRβ double positivity was mostly

associated to juxta-epithelial fibroblasts (high frequency at short distances).

Integrin α11-expressing CAFs promote *in vitro* tumor cell invasion in response to PDGF-BB

The *in vivo* and *silico* studies revealed a strong association between integrin α11 and PDGFRβ in BC stroma. We next performed Western blot analyses on several mouse and human primary cells, and established cell lines: primary mouse PyMT CAFs (mCAFs) and cancer cells (PyMT), primary human breast CAFs (hCAFs), human blood (HUVEC) and lymphatic (HMVEC) endothelial cells, MDA-MB-231, MCF-7 and SKBr3 human BC cells (Supplemental Figure 6A). Both mCAFs and hCAFs showed high integrin α11 expression levels, while other stromal and tumor cells had undetectable levels of this integrin. For functional investigations *in vitro*, two approaches were used: 1) CAFs were isolated from WT (mCAF WT) and KO (mCAF KO) PyMT late carcinomas; 2) ITGA11 expression was downregulated (KD) in WT CAFs issued from PyMT tumors or human BC CAFs through siRNA technology (mCAF/hCAF CTRL and KD). The overall efficiency of integrin knock-down was > 80% (Supplemental Figure 6B). Those different CAF populations were tested for their ability to remodel a collagen matrix and promote cell invasion (Figure 7, A-F and Supplemental Figure 6, C-H). While WT CAFs contracted the collagen lattice to > 80% of its original size, mCAFs KO achieved less than 60% of gel reduction within 96h (Supplemental Figure 6C). Similarly, α11-silenced CAFs (mCAFs and hCAF1 KD) displayed impaired collagen contraction capacity (70% in CTRL mCAF/hCAF1 *vs* 40% in mCAFs KD and 50% in hCAF1 KD) (Supplemental Figure 6, D and E). Next, we evaluated the impact of integrin α11 on CAF invasion in spheroids embedded in a 3D collagen matrix, a model implying ECM remodelling by proteases. Integrin α11-deficiency impaired CAF

invasion into the matrix under basal conditions (Control) (Figure 7, A-C). Interestingly, when stimulated with PDGF-BB, the main ligand of PDGFRβ, mCAFs and hCAF1 showed a strong increase in CAF invasion with a higher degree of response to PDGF-BB for α11-positive CAFs when compared to deficient ones (Figure 7, A-C). These data suggest that α11-negative CAFs are less sensitive to PDGF-BB stimulation than their WT counterpart. These findings were confirmed with three other primary hCAFs (hCAF2-4) issued from hormone-positive or TNBC BC patients (Supplemental Figure 7, A-C).

We next evaluated the impact of integrin α11-positive CAFs on tumor cell invasion upon PDGF-BB stimulation. To address the heterogeneity issues, CAFs were confronted to tumor cells with distinct molecular and invasive properties: mCAFs with PyMT tumor cells (low hormone sensitivity, more invasive) (Figure 7D) or hCAF1-4 with MCF-7 (high hormone sensitivity, less invasive) and MDA-MB-231 cells (hormone insensitivity, more invasive) (Figure 7, E and F, Supplemental Figure 7, D-I). As previously seen in CAF homospheroids, α11-positive CAFs in heterospheroids, were more invasive than α11-deficient ones (Supplemental Figure 6F). Tumor cell confrontation to CAFs in heterospheroids resulted in increased tumor cell invasion as compared to that observed in homospheroids. Moreover, integrin α11-positive CAFs had a higher capacity to promote tumor cell invasion than α11-deficient CAFs (Figure 7, D-F, Supplemental Figure 6G). Importantly, PDGF-BB treatment strongly enhanced tumor cell invasion when tumor cells were confronted to α11-positive CAFs (Figure 7, D-F, Supplemental Figure 6G), but not to α11-deficient CAFs. These data point to the incapacity of α11-deficient CAFs to promote tumor cell invasiveness via PDGF signalling. Of note, while CAFs were sensitive to PDGF-BB stimulation (Figure 7, A-C), tumor cell invasion was not affected by PDGF-BB treatment in homospheroids

(Figure 7, D-F). The invasive promoting effects of CAFs were comparable for all tumor cell types (two human and one murine) and CAFs (four human and one murine) used (Figure 7 and Supplemental Figure 7, D-I).

To investigate whether CAF-derived integrin α11 promotes tumor cell invasion by a direct cell-cell contact or through soluble factor production, we analyzed tumor cell invasion in homospheroids treated with conditioned medium derived from CAFs WT/KO pre-stimulated or not with PDGF-BB (Supplemental Figure 6H). CAF-derived conditioned medium did not improve tumor cell invasion neither in absence, nor in presence of PDGF-BB for both WT and KO CAFs. Thus, α11-positive CAFs require cell-cell contacts or a juxtaposition to tumor cells to promote their invasion.

Integrin α11 promotes the activation of PDGFRβ and JNK downstream signalling

For mechanistic investigation, we evaluated the impact of integrin α11 on PDGFRβ activation and its downstream signalling. We first determined whether integrin α11 takes part of a molecular complex with PDGFRβ by co-immunoprecipitation (Figure 8A). While no α11/PDGFRβ complex was detected under basal conditions, a complex was formed within 5 minutes, peaked at 10 minutes and persisted until 60 minutes upon PDGF-BB stimulation of WT CAFs. Given the key role of CrkII (herein named CRK) as a connector between tyrosine kinase receptors (RTKs), integrins and downstream effectors (39, 40), we searched for CRK in immunoprecipitates. In WT CAFs, a ligand-dependent recruitment of CRK in the complex formed with PDGFRβ was detected 5 minutes after stimulation and maintained concomitantly to the presence of integrin α11. In sharp contrast, the association of CRK in a molecular complex with PDGFRβ was reduced and transient (until 30 minutes) in KO CAFs, while total amount of CRK protein was not modulated when compared to the WT condition (Figure 8A).

Immunofluorescence staining on CAFs revealed integrin α11 clustering at focal adhesions in absence or presence of PDGF-BB stimulation. Under basal conditions, PDGFRβ showed a diffuse distribution within WT and KO CAFs, while it colocalized within α11+ focal adhesions upon PDGF-BB stimulation. KO CAFs displayed diffuse and less organized PDGFRβ staining at the cell surface, even after PDGF-BB treatment (Figure 8B).

We next evaluated integrin α11 implication in PDGFRβ activation and downstream mediator phosphorylation (Figure 9, A and B). In WT CAFs, a robust PDGFRβ phosphorylation was detected after PDGF-BB stimulation, peaking from 5 minutes to 30 minutes and then gradually decreasing by 60 minutes (Figure 9, A and B). The highest difference in PDGFRβ phosphorylation between WT and KO CAFs was seen with Y771, while the classical Y751 residue was not affected by α11-deficiency (Figure 9A, Supplemental Figure 8A). Accordingly, no difference was detected in AKT, ERK or PLCG1 phosphorylations between the two CAF genotypes (Supplemental Figure 8A). A drastic reduction of JNK and SRC phosphorylations was detected in KO cells (Figure 9, A and B). Given CRK interaction with PDGFRβ (Figure 8A), we investigated the phosphorylation of this adaptor molecule at Y221 residue, a negative regulatory site of protein activity (41). Upon PDGF-BB stimulation, CRK was phosphorylated at Y221 in both WT and KO cells, confirming its recruitment by the receptor. Interestingly, CRK inactivation through Y221 phosphorylation and intramolecular folding was more pronounced in KO CAFs, suggesting a reduced CRK activation (Figure 9, A and B). To exclude the implication of PDGFRα, another partner of CRK molecule, we investigated PDGFRα phosphorylation at Y762 residue, the docking site for CRK (42). Upon PDGF-BB stimulation, no increase in Y762 phosphorylation was seen, excluding PDGFRα implication in CRK activation in these cells (Supplemental Figure 8B).

The direct contribution of PDGFRβ in CRK, SRC and JNK phosphorylation in WT cells is further supported by the pharmacological blockade of their phosphorylation with Imatinib, an inhibitor of PDGFRβ kinase activity (Figure 9C and Supplemental Figure 8C). We next investigated a target of PDGFRβ and JNK signalling, the pro-invasive matricellular protein tenascin C (43, 44). Under basal conditions, high amount of tenascin C was produced by WT CAFs, which was strongly promoted by PDGF-BB (Figure 9, D and E). Conversely, KO CAFs produced low amount of tenascin C (Figure 9D), even after PDGF-BB stimulation (Figure 9E). Pharmacological inhibition of PDGFRβ and JNK signalling abolished PDGF-BB-induced tenascin C expression in WT CAFs, without affecting KO CAFs (Figure 9E). To further confirm the relevance of tenascin C, we analysed human BC samples for a triple colocalisation (Figure 10, A-C). Tenascin C, α11 and PDGFRβ were strongly co-expressed, particularly in IDC tumors when compared to normal associated tissues and DCIS (Figure 10A). Tenascin C expression was strongly correlated with the double receptor colocalisation, particularly in IDC HER2 and TNBC subtypes (Figure 10B). Furthermore, we measured the mean distance separating extracellular tenascin C+ areas and α11/PDGFRβ+ regions. An enrichment of tenascin C was detected at the proximity of α11/PDGFRβ+ areas (Figure 10C).

Functional assays in the spheroid model were conducted to validate the implication of PDGFRβ pathway in CAF invasion and CAF-induced tumor cell invasion. Pharmacological inhibition of PDGFRβ and JNK by Imatinib and SP600125, respectively (Figure 11, A and C) blocked PDGF-BB-mediated CAF invasion. Importantly, tumor cell invasion in homospheroids was not affected by PDGFRβ or JNK inhibition (Figure 11, B and D). However, tumor cell invasion in heterospheroids with WT CAFs was completely restored to the control baseline both by PDGFRβ and

JNK inhibition. Collectively, these findings demonstrate that integrin α11-modulated PDGFRβ/JNK signalling in CAFs is an important pathway to promote cancer cell invasiveness.

DISCUSSION

Tumor cells are not self-supporting entities and their metastatic abilities are affected by stromal cells including a heterogeneous population of CAFs. In this study, by using human BC samples and transgenic mice with spontaneous onset of mammary tumors, we identify an integrin α11/PDGFRβ+ CAF subset displaying tumor-promoting features that is associated with a poor clinical outcome. The link between stromal integrin α11 and PDGFRβ has been established at 1) transcriptional level in human BC samples by data mining, 2) histological level in human and murine BC by IHC, 3) cellular level by immunostaining on CAFs, 4) molecular level by co-immunoprecipitation assay, and 5) functional level in *in vitro* assays. Mechanistically, we uncover a role for integrin α11 in regulating PDGFRβ signalling and its downstream JNK activation, which leads to increased expression of one of its targets, tenascin C, a pro-invasive matricellular protein, strongly co-expressed with integrin α11 and PDGFRβ in clinical samples. We provide clear evidence that integrin α11-PDGFRβ molecular crosstalk exploits JNK signalling to endow CAFs with pro-tumorigenic abilities in sustaining the invasiveness of BC cells.

The originality of the present work is to investigate integrin α11, a fibrillar collagen-binding β1 integrin, mainly expressed by fibroblastic cells. Previous studies already reported that this integrin is expressed by mesenchymal cell types in wound healing and lung cancer (29, 32, 33). Whether integrin α11 expression is restricted or not to a specific CAF subset was not yet documented. Our study highlights that integrin α11 expression is mostly localised in the stromal compartment of BC and provides evidence for a strong association between integrin α11 and PDGFRβ, both in clinical BC samples and in the pre-clinical PyMT mouse model. High *PDGFRB* expression has already been correlated with shorter patient survival and this molecule is proposed as

a prognostic marker in many cancer types including BC (23, 45, 46). Here, Kaplan-Meyer analysis revealed that high *ITGA11* expression is correlated with lower overall and metastasis-free survivals of patients with BC. Additionally, integrin α11/PDGFRβ colocalisation was associated to a poor outcome, including high proliferation rate and histological grade, as well as increased metastasis and mortality. The integrin α11/PDGFRβ co-expression was denser in invasive tumors and mostly confined to the juxta-epithelial fibroblasts. Due to technical limitation related to the lack of anti-α11 integrin antibody suitable on paraffin sections, our IHC study was restricted to frozen BC samples and is worth extending into larger cohorts. Our data are in line with a recent study showing that PDGFRβ+ peritumoral fibroblasts constitute a poor prognosis-associated CAF subset for high-risk of recurrence in DCIS (47). In agreement with the clinical data, *Itga11*-deficiency in mice drastically delayed PyMT tumor growth and reduced lung metastasis. Altogether, these findings indicate that integrin α11 exerts a tumor-promoting function and is mostly expressed by a subtype of PDGFRβ+ CAFs. However, we cannot exclude the possibility that integrin α11 displays additional pro-tumoral features in a PDGFRβ-independent manner. Indeed, in both human and murine tumor samples, the α11/PDGFRβ+ CAF subset represents around 70% of α11+ CAFs, with a remaining population of 30% of α11+/PDGFRβ- CAFs. The moderate increase of the pro-invasive activity of α11+ CAFs observed under basal conditions (without PDGF-BB) suggests that this integrin might also be involved in other pro-tumoral effects.

The desmoplastic reaction represents a feature of disease malignancy and patient outcome in human BC (48). Our data mining revealed that *ITGA11* expression strongly correlates with several fibroblastic markers and collagen molecules in human BC, further confirming an association between this integrin with CAFs and the desmoplastic

reaction. Moreover, PDGF signalling was also linked to desmoplasia initiation in human BC (49), which additionally supports the synergistic crosstalk between integrin α11 and PDGFRβ. Interestingly, *ITGA11* upregulation that we initially found in human BC, was confirmed in other desmoplastic cancers including lung, pancreas, colorectal and gastric cancers. It is worth mentioning that the second fibrillar collagen-binding α2β1 integrin (*ITGA2*) is downregulated in human BC and acts as a metastasis suppressor in a murine model (50). These data suggest opposite effects of the two fibrillar collagen-binding integrins (α2β1 and α11β1) in BC.

Although PDGFRβ is a well-known marker of pericytes (19), integrin α11+ cell subset is unlikely to be a pericyte subpopulation, as α11 integrin positivity poorly correlates with αSMA or NG2. Additionally, the absence of an association between α11 and FSP1 positivity suggests that α11+ cells are distinct from normal fibroblasts, as FSP1 was proposed as a marker of quiescent tissue fibroblasts (4) and is poorly expressed in late stage PyMT tumors used in this study. The slight association between integrin α11 and FAP (22%) might reflect a partial overlap of FAP, PDGFRβ and β1 integrin+ CAF subsets as previously reported (12). Given the multiple putative cellular source of CAFs, it is possible that other host α11+ cells than resident fibroblasts contribute to tumor growth. This possibility was excluded by transplanting WT tumors into KO-mice leading to similar tumor growth than in WT mice. This clearly demonstrates that tumor resident α11+ cells are sufficient for the observed pro-tumoral effects.

A key finding of our study is the ligand-dependent interaction of PDGFRβ with integrin α11 assessed by co-immunoprecipitation and immunofluorescence studies. Importantly, the two proteins colocalized at focal adhesions. Along with the classical integrin-ECM signalling, integrin-RTK crosstalk is already documented for several RTKs including EGFR, IGFR, FGFR, PDGFR or Met receptors (26, 51). Integrins can

promote RTK phosphorylation and/or amplify their intracellular signalling. In this context, clustering of cell surface β1 integrins has been reported to induce PDGFRβ phosphorylation (25). In our system, upon ligand-induced interaction of PDGFRβ with integrin α11, we observed an increase of receptor phosphorylation, suggesting a collaborative signalling between this RTK and integrin α11 (26). When considering downstream mediators of PDGFRβ signalling, we observed a modulation of CRK, SRC and JNK phosphorylations. CRK and SRC implication in integrin signalling is widely described (52, 53). PDGFRβ is known to bind and phosphorylate CRK adaptor molecule (42). Accordingly, our data demonstrate that α11-PDGFRβ interaction is associated with CRK recruitment assessed by co-immunoprecipitation assay, as well as SRC and JNK activation (Graphical abstract). The absence of integrin α11 does not prevent the formation of CRK/PDGFRβ complex but increases CRK phosphorylation at Y221, the negative regulator site of its activity. Pharmacological inhibition of PDGFRβ by Imatinib, altered the phosphorylation of CRK, SRC and JNK. Thus, integrin α11 interaction with PDGFRβ likely favours JNK downstream signalling, rather than classical ERK or AKT pathways. The involvement of additional molecular partners/pathways cannot be excluded.

PDGFRβ or JNK pharmacological inhibition impaired not only CAF invasion, but most importantly the invasiveness of cancer cells in mixed spheroids. Of note, cancer cells themselves are not sensitive to PDGF-BB stimulation, further highlighting the contribution of integrin α11 in CAF-cancer cell crosstalk. An important finding is that α11+ CAFs issued either from mice or from human patients (four different subpopulations) were all able to promote tumor cell invasion, independently of intrinsic tumor cell properties. Therefore, α11+ CAFs display a pro-invasive activity on tumor cells, and the extent of this effect might be tumor cell-dependent.

The tumor-promoting capacities of CAFs have been widely described as being related to their secretome and ability to remodel the extracellular matrix (4). Our study demonstrates that integrin α11+ CAFs promote cancer cell invasion in a cell-cell contact or a proximal manner. This process could imply the local production of growth factors, migratory modulators, matrix molecules and/or involve matrix remodelling (54). Integrins have been shown to mediate CAF-induced invasion of cancer cells, by generating tracks within the matrix through the combined action of force- and protease-mediated matrix remodelling (14). Our study provides evidence that the crosstalk between integrin α11 and PDGFRβ and subsequent JNK activation contribute to the acquisition of CAF pro-tumorigenic abilities. The integrin α11/PDGFRβ/JNK molecular axis results in changes in ECM composition with increased deposition of at least one pro-invasive matricellular protein (tenascin C). Previous studies have clearly documented that fibroblast-derived tenascin C is a key matricellular protein that promotes tumor cell invasion (14, 55, 56). Of note, its increased expression in tumors is associated with disease progression and metastasis (57). In line with our data, both PDGF and JNK signalling pathways have been reported to regulate tenascin C expression (43, 44). Moreover, our study reveals a strong association between α11/PDGFRβ+ CAFs and tenascin C expression, particularly in IDC, more aggressive BC molecular subtypes. Although tenascin C regulation contributes to the pro-invasive effects exerted by CAFs on tumor cells, we cannot exclude the putative involvement of proteases and other pro-invasive ECM molecules in this model.

Collectively, our work sheds a new light on the role played by integrin α11 in BC stroma. This integrin associates mainly to PDGFRβ in a CAF subset displaying tumor-promoting and pro-metastatic potentials. We identify integrin α11/PDGFRβ/JNK axis as an important mediator of CAF-promoted tumor invasiveness. Pharmacological

approaches targeting such molecular partnership may have strong implications in cancer treatment and prediction of patient response to RTK treatments.

METHODS

Generation of *Itga11*-deficient MMTV-PyMT mouse model

Itga11 knockout mice (Itga11^{tm1Dgul}) (35) were backcrossed into a FVB/N background (Harlan, the Netherlands) for six generations, and then crossed with MMTV-PyMT FVB/N transgenic mice expressing Polyoma Middle T antigen oncogene under Mouse Mammary Tumour Virus promoter (Tg(MMTV-PyVT)634Mul) for six generations (34). All animals were kept within the accredited Mouse Facility and Transgenics GIGA platform of University of Liège (Belgium) in specific pathogen-free conditions. Genotyping was performed by PCR of tail genomic DNA as described (58). Primers sequences for *Itga11* and PyMT are presented in Supplemental Table 4. Tumor growth was assessed by measuring the tumor volume (V = length × width^2 × 0.4) twice a week and the tumor mass at sacrifice. Tumor measurement started at week 5 after birth until week 14 for WT and KO groups. For KO late group, *Itga11*-deficient mice were left longer than 14 weeks (maximum until week 18), until they reached the same tumor volume as WT mice at 14 weeks.

For transplantation experiments, matched WT PyMT tumors (11 weeks-old, 2 mm-sized fragments) were engrafted into fat pads of FVB/N *Itga11* WT or KO mice (aged 10-12 weeks) and tumor volumes were estimated twice a week.

Cell isolation from mouse and human samples

Mouse CAFs (mCAF) and PyMT tumor cells (PyMT) were isolated from PyMT mice as described (59). Late carcinoma tumor samples were surgically removed at week 14. Samples were cut into small pieces and enzymatically digested with a collagenase solution for 45 min at 37°C (Collagenase Type IA, Clostridium histolyticum, Sigma Aldrich, Belgium). After filtration and centrifugation of cell suspension, the pellet was

washed, re-suspended and cultured in medium defined below. Cells were plated for 30 min to let fibroblasts adhere. The supernatant containing tumor cells was then removed and plated in a separate flask. All PyMT tumor cells were positive for cytokeratin. Primary cultured CAFs were used at early passages (until passage 5 and for no longer than 14 days of culture). CAFs were positive for vimentin and negative for cytokeratin. Human CAFs (hCAF), isolated in a similar way, were derived from women undergoing a mammectomy with following tumor characteristics: hCAF1 (99 % estrogen receptor+, 25 % progesteron receptor+ and HER2-), hCAF2 (95 % estrogen and progesterone receptors+ and HER2-), hCAF3 and hCAF4 (triple negative). Primary cells were isolated by preparing a single cell suspension from tumor fragments (1-3 mm^3) followed by culture plate adherent passaging. They were positive for vimentin (100 %) and negative for cytokeratin. Primary hCAF2-4 were used until passage 4. The hCAF1 were immortalized after infection with a pBABE retroviral vector expressing the hTERT open reading frame (hTERT hCAF1) and used until passage 8.

Cell culture and siRNA transfection

CAFs and PyMT tumor cells, human BC cell lines (MCF-7, MDA-MB-231 and SKBr3, obtained from ATCC, USA) were cultured in DMEM (Gibco, ThermoFisher) supplemented with 10% FBS, L-Glutamine (2 mM), penicillin (100 u/ml) and streptomycin (100 µg/ml) at 37°C and humidified 5% CO_2 atmosphere, until reaching 90–100% of confluency. Human primary blood (HUVEC) and lymphatic (HMVEC-D) endothelial cells were cultured in EGM2 and EGM2-MV medium (Lonza, Verviers, Belgium), respectively. All cells were mycoplasma-free. All human cell lines described above were authenticated before use (Leibniz-Institute DSMZ, Germany). For *ITGA11/Itga11* downregulation, cells at 60-70% of confluency were transfected for 48

h prior experiments with Interferin siRNA transfection reagent (Polyplus, France) and Mouse or Human SMARTpool: ON-TARGETplus *Itga11* siRNA (Dharmacon) (20 nM) in DMEM supplemented with 10% FBS. ON-TARGETplus Non-targeting Control Pool (Dharmacon) was used as negative transfection control. *ITGA11/Itga11* downregulation was confirmed after 48-72 h by Western blot. For Western blot and co-immunoprecipitation experiments, cells were used at 90-100% of confluency after 3 days of seeding. For immunofluorescence confocal detection, low confluency cells (20-30%) were used 20 h after seeding. For PDGF-BB stimulation, high-confluency cells were serum-starved for 2 h, followed by PDGF-BB stimulation (R&D Systems) (10 ng/ml). For Imatinib experiment, high-confluency cells were serum-starved for 2 h and pre-treated with Imatinib (LC Laboratories, USA) (5 µM) for 1.5 h followed by PDGF-BB stimulation.

Bioinformatics analysis

Meta-analysis of global gene expression data in the Oncomine database (60) (Compendia Bioscience, Ann Arbor, USA) was performed using primary filters for “breast cancer” and “cancer *vs* normal analysis”, sample filter to use “clinical specimens” and data type filter to use “mRNA” data sets (8 datasets representing 2415 patients). Patients of all ages, gender, disease stages or treatments were included. Data were acquired in an unbiased manner by compiling all the Oncomine studies with significantly altered ITGA11 expression at the threshold settings (*P*-value = 0.05, fold-change = 1.5, and gene rank = all) (60). Significant studies, in which at least one analysed group was comprised of three patients or less were excluded. All data are reported as $\log_2$ median-centered intensity in the Oncomine database. The datasets were exported from Oncomine and analysed in GraphPad Prism V7 software.

The gene expression profile of GSE8977 (61), GSE9014 (62), GSE14548 (63), GSE33692 (64), GSE41228 (36), GSE68744 (65) were obtained from the NCBI Gene Expression Omnibus (GEO) database (66) and data were recalculated using the GEO2R analytical tool (67). The log_2 transformed expression values of *ITGA11* were exported from GEO2R and analysed in GraphPad Prism. Identification of genes whose expression profiles were best correlated with *ITGA11* mRNA levels was performed by interrogating gene expression datasets contained at cBioPortal and Breast Cancer Gene-Expression Miner (bc-GenExMiner). bc-GenExMiner contains 36 datasets including 5861 breast cancer patients (68). cBioPortal was used to explore the TCGA breast (69) and Metabric (70) cohorts. For each of these three patient cohorts (referred to as TCGA, Metabric and GenExMiner), genes with Pearson's correlation coefficients > 0.5 were selected and classified as being *ITGA11*-co-expressed genes. The intersections of co-expressed genes from the 3 cohorts were analysed using Venny 2.1 online tool. Kaplan–Meier curves were generated with Kaplan-Meier plotter website, using a database of public microarray datasets (71). Automatic cut-off scores were selected during queries, overall survival (OS) and distant metastasis free survival (DMFS) were selected. Log-rank *P*-values were computed as described (71). Integrative co-expression network was analysed in TCSBN database as previously described (38).

Histological analysis

Mouse tumor and lung samples were formalin fixed (4%) and paraffin embedded. Sections of 6 µm thickness were counterstained with haematoxylin & eosin and mounted with Eukitt medium for light microscope observation. For desmoplasia analysis, a Van Gieson staining was performed by incubating slides with Weigert's iron

hematoxylin solution, followed by Van Gieson staining (Sigma Aldrich, Bornem, Belgium). Slides were scanned using the NanoZoomer 2.0-HT system (Hamamatsu, Belgium) and automatic quantification was performed with the image analysis toolbox of MATLAB 8.3 software (MathWorks Inc., USA). Desmoplasia was expressed as collagen density normalized to total tumor area. For metastasis quantification, 6 lung sections at distance of 10 of 6 µm were analysed for each mouse. Metastatic index was calculated by dividing the tumor lung area to the total lung area.

Immunofluorescence studies

For colocalisation studies on mouse samples, cryosections embedded in OCT (6 µm thickness) were fixed in acetone at -20°C for 10 min, followed by rehydration and blocking in Protein Block, Serum-Free Solution (Dako, Agilent) for 10 min. Primary and secondary antibodies (references and dilutions in Supplemental Table 5) were incubated sequentially in Antibody Diluent with Background Reducing Components (Dako, Agilent). Slides were mounted in DAPI Fluoromount-G (SouthernBiotech) and analysed within 48 h after staining. For integrin α11 and PDGFRβ colocalisation on human samples, cryosections of human carcinoma and the associated normal breast tissues were analysed for the following groups: ductal carcinoma in situ (DCIS) and invasive ductal carcinomas (IDC) of luminal A and B, HER2 and TNBC cancers (68 patients). For detection of integrin α11 on human samples, the anti-human Mab203E1H5 antibody was produced (Gullberg et al, in preparation) (antibody deposed under Patent Application European Patent Office-EP18155716). All samples were analysed by confocal Olympus Fluoview 1000 microscopy in Kalman filter mode with 20X-magnification objective. For image analysis and quantification, protein expression hotspots were identified within tumor sections (at least 6 stromal

fields/sample) and integrin α11, PDGFRβ and colocalisation densities were quantified by specifically-designed algorithm in MATLAB 8.3 software. The proximity analysis was performed by identifying the Euclidean distance from each pixel belonging to integrin α11+, PDGFRβ+ and colocalised+ areas to tumor nodules. Pictures lacking defined tumor areas were excluded. For triple colocalisation, the proximity of tenascin C to the colocalised integrin α11/PDGFRβ areas was calculated as described above. For immunofluorescence studies on CAFs, low-confluency cells (20-30%) were fixed in methanol/acetone mixture (80/20) at -20°C for 10 min, followed by rehydration and blocking in Innovex Background Buster (Innovex Biosciences, USA) for 10 min. Cells were incubated with primary and secondary antibodies as described above. Samples were analysed by confocal Olympus Fluoview 1000 microscopy in Kalman filter mode with 60x-magnification oil immersion objective.

Collagen contraction assay

For each replicate, 2 x 10^5 cells were suspended in 700 µl of native collagen solution (2 mg/ml) buffered at pH = 7.5 (rat tail Collagen I, Corning) and seeded in a 12-well plate pre-treated with 2% BSA solution. After collagen polymerisation at 37°C, gels were detached carefully from well border and medium supplemented with 5% of FBS was added. Collagen lattice contraction was monitored for 96 h, by taking pictures daily with a LAS-4000 image analyser (Fujifilm, Belgium). Gel area was measured by ImageJ NIH software and the % of gel reduction was calculated by subtracting the gel area for each day from the gel area at time 0 h.

Spheroid invasion assay

For fluorescence cell tracking, CAFs and tumor cells were incubated for 30 min in serum-free medium with CellTracker Green CMFDA or Orange CMRA (Invitrogen, Thermo Fisher). Spheroids were prepared by seeding 500 CAFs or 1000 tumor cells (homospheroids) or a mixture of both (heterospheroids) in 200 µl of DMEM supplemented with 10% FBS and containing 20% of carboxymethylcellulose 4000 cp (Sigma Aldrich). Cells were seeded in round bottom non-adherent 96-well plates (CellStar, Greiner BioOne) for 24 h for spheroid formation. The following day, single spheroids were collected from wells, centrifuged and suspended in 500 µl/well of native collagen solution (2 mg/ml) (rat tail Collagen I, Corning) at pH 7.5 and seeded in collagen pre-coated 12-well plates (15 spheroids/well; 2 wells/condition). After collagen polymerization, 500 µl of DMEM supplemented with 2% FBS was carefully added. For PDGF-BB stimulation, spheroids were treated with recombinant human PDGF-BB (R&D Systems) (10 ng/ml). In some assays, Imatinib (LC Laboratories, USA) and SP600125 (Sigma Aldrich) were added (5 µM). Spheroids were analysed after 20 h of culture and image acquisition was performed by epifluorescence Nikon Eclipse Ti microscope (10x-magnification objective). Image analysis was performed as described (72). Cell invasion was automatically quantified by specifically-designed algorithm in MATLAB 8.3 software. Data were expressed as the maximal distance of cell invasion from the spheroid border.

RNA extraction and RT-qPCR analysis

Total tumor RNA was extracted using the RNeasy Mini Kit (Qiagen GmbH, Germany). RNA was quantified and purity checked with the ND-1000 NanoDrop spectrophotometer (Nanodrop Technologies, USA). RT-qPCR was performed on

reverse transcribed RNA (First Strand cDNA Synthesis kit, Roche) with LightCycler480 Probes Master kit (Roche) and the Universal Probe Library system (Roche) using specific primers (Eurogentec, Belgium). Data were normalized to mouse TBP. Primer nucleotide sequences are indicated in Supplemental Table 4.

Western blot and co-immunoprecipitation analysis

For protein extraction, frozen tumor samples or fresh cells were suspended in Lysis Buffer (Cell Signalling Technology) supplemented with Complete protease and PhoStop phosphatase inhibitor cocktails (Roche). Tumor samples were homogenized with the MagnaLyser system (Roche), while cell samples were scraped on ice. After centrifugation at 14000 g for 10 min at 4°C, proteins were quantified with the DC protein assay kit (Bio-Rad Laboratories, USA). Tumor (100 µg) or cell extracts (20 µg) were separated by SDS-PAGE under reducing conditions. PVDF membranes (NEN, USA) were incubated for 1 h in 5% non-fat dry milk or BSA PBS solution, followed by overnight incubation with primary antibodies. Antibodies and dilutions are indicated in Supplemental Table 5. Immunocomplexes were detected with an enhanced chemiluminescence ECL-Plus® system and visualized with image analyzer (LAS-4000; Fujifilm, Belgium). Band densities were quantified with Quantity-One software (BioRad Laboratories). For loading control, membranes were incubated with HSC-70 antibody. For phosphorylation experiments, membranes were stripped in Restore Western Blot Stripping Buffer (ThermoFisher), re-blocked and re-incubated with antibodies for total protein detection. For co-immunoprecipitation analysis, 700 µg of protein extracts were immunoprecipitated overnight with PDGFRβ antibody (clone 2B3, Cell Signalling Technology) according to manufacturer's instructions. Protein complexes were re-suspended in Dynabeads Protein G solution (50 µl)

(ThermoFisher) and incubated for 8 h, at 4°C. Protein-bead complexes were collected from a magnet system, washed and re-suspended in Lysis Buffer and heated for 5 min at 95°C. Samples were next analysed by Western blot. Total protein extracts, CAF KO, IgG and input samples were used as immunoprecipitation controls.

Statistical analysis

Unless otherwise stated, statistical analysis was performed with SigmaPlot and GraphPad Prism softwares and results were expressed as mean ± SEM. For 2-group comparison, 2-tailed unpaired t test or Mann-Whitney test were performed. For multiple group comparison, 1-way ANOVA or Kruskall-Wallis tests were performed with the multiple comparison post hoc correction as indicated. The equality of variance between groups and Normality Shapiro-Wilk test were performed and statistical tests were chosen accordingly. Graphs show the exact *P* value or star symbols (ns = not significant; *$P < 0.05$; ** $P < 0.01$; *** $P < 0.001$; **** $P < 0.0001$). A $P < 0.05$ was considered significant.

Study approval

All animal experiments were conducted at the GIGA Animal Facility of ULiège (Belgium) in accordance with the Federation of European Laboratory Animal Science Associations (FELASA) and local ethical committee at ULiège. Cryosections of human BC samples and related normal associated tissues (n = 68 including 11 DCIS, 14 IDC luminal A, 17 IDC luminal B, 11 IDC HER2 and 15 IDC TNBC) were provided by the Biobank of the University Hospital of Liège (Belgium) for a retrospective study in accordance with the current legislation and recommendations of the Ethical Committee of the University Hospital of Liège.

Author Contributions:

P. I.: established *Itga11*-/- MMTV-PyMT mice, designed, performed and analysed all experiments, wrote the manuscript; **M. E.**: conducted *in silico* data analysis and wrote the manuscript; **B. S. and L. T.**: performed all computerized quantification; **C. A.**: contributed to *Itga11* PyMT mice breeding; **S. H.** and **S. L.**: contributed to immunostainings; **D. J.** and **W. O.**: provided hCAFs and contributed to data interpretation; **S. NE., P. C** and **C. D.** participated at experiment design and data interpretation; **H. R** and **P. T**. established and provided the *Itga11*-/- FVB/N mice; **G. D.**: contributed to data interpretation and provided ITGA11 tools; **N. A.**: supervised, funded, designed the project, interpreted the data and wrote the manuscript.

Acknowledgements:

We thank all laboratory members for useful technical advice, and all members of Marie Curie CAFFEIN ITN network for valuable scientific discussions. We thank GIGA Imaging and Animal facility platforms of ULiège for technical support and mouse housing. We thank the Biobank of ULiège for providing BC samples.

This project was part of the CAFFEIN FP7 ITN consortium and received funding from the People Program (Marie Curie Actions) of the European Union's Seventh Framework Program FP7/2007-2013/under REA grant agreement n° [316610]. The opinion presented in the current article reflects only the author's view and that the Union is not liable for any use that may be made of the information contained therein.

Conflict of interest

For Mab203E1H5 antibody Gullberg D. is a named inventor on a patent filed by the University of Bergen, Norway.

Funding

This work was supported by grants from ITN Marie Curie Actions FP7/2007-2013/ grant agreement n°316610, the Fonds de la Recherche Scientifique - FNRS (F.R.S.-FNRS, Belgium), the Fondation contre le Cancer (foundation of public interest, Belgium), the Fonds spéciaux de la Recherche (University of Liège), the Fondation Hospital-Universitaire Léon Frédéricq (University of Liège), the Research Council of Norway through its Centres of Excellence funding scheme (project number 223250), the Academy of Finland research council for Health (grant 308867) and the Sigrid Jusélius Foundation, IUAP Belspo. Canale A. and Louis T. are supported by FNRS-Televie fellowships. Maquoi E. is a Research Associate from FNRS (Belgium).

REFERENCES

1. Pan H, et al. 20-Year Risks of Breast-Cancer Recurrence after Stopping Endocrine Therapy at 5 Years. *The New England journal of medicine.* 2017;377(19):1836-46.

2. Hanahan D, and Coussens LM. Accessories to the crime: functions of cells recruited to the tumor microenvironment. *Cancer cell.* 2012;21(3):309-22.

3. Orimo A, and Weinberg RA. Heterogeneity of stromal fibroblasts in tumors. *Cancer biology & therapy.* 2007;6(4):618-9.

4. Kalluri R. The biology and function of fibroblasts in cancer. *Nature reviews Cancer.* 2016;16(9):582-98.

5. LeBleu VS, and Kalluri R. A peek into cancer-associated fibroblasts: origins, functions and translational impact. *Dis Model Mech.* 2018;11(4).

6. Sun KH, Chang Y, Reed NI, and Sheppard D. alpha-Smooth muscle actin is an inconsistent marker of fibroblasts responsible for force-dependent TGFbeta activation or collagen production across multiple models of organ fibrosis. *American journal of physiology Lung cellular and molecular physiology.* 2016;310(9):L824-36.

7. Ohlund D, Elyada E, and Tuveson D. Fibroblast heterogeneity in the cancer wound. *The Journal of experimental medicine.* 2014;211(8):1503-23.

8. Gascard P, and Tlsty TD. Carcinoma-associated fibroblasts: orchestrating the composition of malignancy. *Genes & development.* 2016;30(9):1002-19.

9. Hanahan D, and Weinberg RA. Hallmarks of cancer: the next generation. *Cell.* 2011;144(5):646-74.

10. Orimo A, et al. Stromal fibroblasts present in invasive human breast carcinomas promote tumor growth and angiogenesis through elevated SDF-1/CXCL12 secretion. *Cell.* 2005;121(3):335-48.

11. Erez N, Truitt M, Olson P, Arron ST, and Hanahan D. Cancer-Associated Fibroblasts Are Activated in Incipient Neoplasia to Orchestrate Tumor-Promoting Inflammation in an NF-kappaB-Dependent Manner. *Cancer cell.* 2010;17(2):135-47.

12. Costa A, et al. Fibroblast Heterogeneity and Immunosuppressive Environment in Human Breast Cancer. *Cancer cell.* 2018;33(3):463-79 e10.

13. Zhang D, et al. Metabolic reprogramming of cancer-associated fibroblasts by IDH3alpha downregulation. *Cell reports.* 2015;10(8):1335-48.

14. Gaggioli C, et al. Fibroblast-led collective invasion of carcinoma cells with differing roles for RhoGTPases in leading and following cells. *Nature cell biology.* 2007;9(12):1392-400.

15. De Vlieghere E, Verset L, Demetter P, Bracke M, and De Wever O. Cancer-associated fibroblasts as target and tool in cancer therapeutics and diagnostics. *Virchows Archiv : an international journal of pathology.* 2015;467(4):367-82.

16. Ozdemir BC, et al. Depletion of carcinoma-associated fibroblasts and fibrosis induces immunosuppression and accelerates pancreas cancer with reduced survival. *Cancer cell.* 2014;25(6):719-34.

17. Rhim AD, et al. Stromal elements act to restrain, rather than support, pancreatic ductal adenocarcinoma. *Cancer cell.* 2014;25(6):735-47.

18. Roswall P, et al. Microenvironmental control of breast cancer subtype elicited through paracrine platelet-derived growth factor-CC signalling. *Nature medicine.* 2018;24(4):463-73.

19. Ostman A. PDGF receptors in tumor stroma: Biological effects and associations with prognosis and response to treatment. *Advanced drug delivery reviews.* 2017;121:117-23.

20. Frings O, et al. Prognostic significance in breast cancer of a gene signature capturing stromal PDGF signalling. *The American journal of pathology.* 2013;182(6):2037-47.

21. Ostman A, and Heldin CH. PDGF receptors as targets in tumor treatment. *Advances in cancer research.* 2007;97:247-74.

22. Paulsson J, et al. High expression of stromal PDGFRbeta is associated with reduced benefit of tamoxifen in breast cancer. *The journal of pathology Clinical research.* 2017;3(1):38-43.

23. Paulsson J, et al. Prognostic significance of stromal platelet-derived growth factor beta-receptor expression in human breast cancer. *The American journal of pathology.* 2009;175(1):334-41.

24. Yamada KM, and Even-Ram S. Integrin regulation of growth factor receptors. *Nature cell biology.* 2002;4(4):E75-6.

25. Sundberg C, and Rubin K. Stimulation of beta1 integrins on fibroblasts induces PDGF independent tyrosine phosphorylation of PDGF beta-receptors. *The Journal of cell biology.* 1996;132(4):741-52.

26. Ivaska J, and Heino J. Cooperation between integrins and growth factor receptors in signalling and endocytosis. *Annual review of cell and developmental biology.* 2011;27:291-320.

27. Zeltz C, Lu N, and Gullberg D. Integrin alpha11beta1: a major collagen receptor on fibroblastic cells. *Advances in experimental medicine and biology.* 2014;819:73-83.

28. Barczyk MM, Lu N, Popova SN, Bolstad AI, and Gullberg D. alpha11beta1 integrin-mediated MMP-13-dependent collagen lattice contraction by fibroblasts: evidence for integrin-coordinated collagen proteolysis. *Journal of cellular physiology.* 2013;228(5):1108-19.

29. Zeltz C, and Gullberg D. The integrin-collagen connection--a glue for tissue repair? *Journal of cell science.* 2016;129(4):653-64.

30. Carracedo S, et al. The fibroblast integrin alpha11beta1 is induced in a mechanosensitive manner involving activin A and regulates myofibroblast differentiation. *The Journal of biological chemistry.* 2010;285(14):10434-45.

31. Schulz JN, et al. Reduced granulation tissue and wound strength in the absence of alpha11beta1 integrin. *The Journal of investigative dermatology.* 2015;135(5):1435-44.

32. Zhu CQ, et al. Integrin alpha 11 regulates IGF2 expression in fibroblasts to enhance tumorigenicity of human non-small-cell lung cancer cells. *Proceedings of the National Academy of Sciences of the United States of America.* 2007;104(28):11754-9.

33. Navab R, et al. Integrin alpha11beta1 regulates cancer stromal stiffness and promotes tumorigenicity and metastasis in non-small cell lung cancer. *Oncogene.* 2016;35(15):1899-908.

34. Guy CT, Cardiff RD, and Muller WJ. Induction of mammary tumors by expression of polyomavirus middle T oncogene: a transgenic mouse model for metastatic disease. *Molecular and cellular biology.* 1992;12(3):954-61.

35. Popova SN, et al. Alpha11 beta1 integrin-dependent regulation of periodontal ligament function in the erupting mouse incisor. *Molecular and cellular biology.* 2007;27(12):4306-16.

36. Lee S, et al. Differentially expressed genes regulating the progression of ductal carcinoma in situ to invasive breast cancer. *Cancer research.* 2012;72(17):4574-86.

37. Croft D, et al. Reactome: a database of reactions, pathways and biological processes. *Nucleic acids research.* 2011;39(Database issue):D691-7.

38. Lee S, et al. TCSBN: a database of tissue and cancer specific biological networks. *Nucleic acids research.* 2018;46(D1):D595-D600.

39. Sorokin A, Reed E, Nnkemere N, Dulin NO, and Schlessinger J. Crk protein binds to PDGF receptor and insulin receptor substrate-1 with different modulating effects on PDGF- and insulin-dependent signalling pathways. *Oncogene.* 1998;16(19):2425-34.

40. Bell ES, and Park M. Models of crk adaptor proteins in cancer. *Genes & cancer.* 2012;3(5-6):341-52.

41. Antoku S, and Mayer BJ. Distinct roles for Crk adaptor isoforms in actin reorganization induced by extracellular signals. *Journal of cell science.* 2009;122(Pt 22):4228-38.

42. Matsumoto T, et al. Differential interaction of CrkII adaptor protein with platelet-derived growth factor alpha- and beta-receptors is determined by its internal tyrosine phosphorylation. *Biochemical and biophysical research communications.* 2000;270(1):28-33.

43. Islam MS, et al. PDGF and TGF-beta promote tenascin-C expression in subepithelial myofibroblasts and contribute to intestinal mucosal protection in mice. *British journal of pharmacology.* 2014;171(2):375-88.

44. Insua-Rodriguez J, et al. Stress signalling in breast cancer cells induces matrix components that promote chemoresistant metastasis. *EMBO molecular medicine.* 2018;10(10).

45. Weissmueller S, et al. Mutant p53 drives pancreatic cancer metastasis through cell-autonomous PDGF receptor beta signalling. *Cell.* 2014;157(2):382-94.

46. Frodin M, et al. Perivascular PDGFR-beta is an independent marker for prognosis in renal cell carcinoma. *British journal of cancer.* 2017;116(2):195-201.

47. Strell C, et al. Impact of Epithelial-Stromal Interactions on Peritumoral Fibroblasts in Ductal Carcinoma in Situ. *Journal of the National Cancer Institute.* 2019.

48. Nazari SS, and Mukherjee P. An overview of mammographic density and its association with breast cancer. *Breast cancer (Tokyo, Japan).* 2018;25(3):259-67.

49. Shao ZM, Nguyen M, and Barsky SH. Human breast carcinoma desmoplasia is PDGF initiated. *Oncogene.* 2000;19(38):4337-45.

50. Ramirez NE, et al. The alpha(2)beta(1) integrin is a metastasis suppressor in mouse models and human cancer. *The Journal of clinical investigation.* 2011;121(1):226-37.

51. Hamidi H, and Ivaska J. Every step of the way: integrins in cancer progression and metastasis. *Nature reviews Cancer.* 2018.

52. Giancotti FG, and Ruoslahti E. Integrin signalling. *Science (New York, NY).* 1999;285(5430):1028-32.

53. Seguin L, Desgrosellier JS, Weis SM, and Cheresh DA. Integrins and cancer: regulators of cancer stemness, metastasis, and drug resistance. *Trends in cell biology.* 2015;25(4):234-40.

54. Desgrosellier JS, and Cheresh DA. Integrins in cancer: biological implications and therapeutic opportunities. *Nature reviews Cancer.* 2010;10(1):9-22.

55. De Wever O, et al. Tenascin-C and SF/HGF produced by myofibroblasts in vitro provide convergent pro-invasive signals to human colon cancer cells through RhoA and Rac. *FASEB journal : official publication of the Federation of American Societies for Experimental Biology.* 2004;18(9):1016-8.

56. Xia S, et al. Tumor microenvironment tenascin-C promotes glioblastoma invasion and negatively regulates tumor proliferation. *Neuro-oncology.* 2016;18(4):507-17.

57. Lowy CM, and Oskarsson T. Tenascin C in metastasis: A view from the invasive front. *Cell adhesion & migration.* 2015;9(1-2):112-24.

58. Popova SN, et al. The mesenchymal alpha11beta1 integrin attenuates PDGF-BB-stimulated chemotaxis of embryonic fibroblasts on collagens. *Developmental biology.* 2004;270(2):427-42.

59. Calvo F, et al. Mechanotransduction and YAP-dependent matrix remodelling is required for the generation and maintenance of cancer-associated fibroblasts. *Nature cell biology.* 2013;15(6):637-46.

60. Rhodes DR, et al. ONCOMINE: a cancer microarray database and integrated data-mining platform. *Neoplasia (New York, NY).* 2004;6(1):1-6.

61. Karnoub AE, et al. Mesenchymal stem cells within tumour stroma promote breast cancer metastasis. *Nature.* 2007;449(7162):557-63.

62. Finak G, et al. Stromal gene expression predicts clinical outcome in breast cancer. *Nature medicine.* 2008;14(5):518-27.

63. Ma XJ, Dahiya S, Richardson E, Erlander M, and Sgroi DC. Gene expression profiling of the tumor microenvironment during breast cancer progression. *Breast cancer research : BCR.* 2009;11(1):R7.

64. Knudsen ES, et al. Progression of ductal carcinoma in situ to invasive breast cancer is associated with gene expression programs of EMT and myoepithelia. *Breast cancer research and treatment.* 2012;133(3):1009-24.

65. Oh EY, et al. Extensive rewiring of epithelial-stromal co-expression networks in breast cancer. *Genome biology.* 2015;16:128.

66. Barrett T, et al. NCBI GEO: archive for functional genomics data sets--update. *Nucleic acids research.* 2013;41(Database issue):D991-5.

67. Davis S, and Meltzer PS. GEOquery: a bridge between the Gene Expression Omnibus (GEO) and BioConductor. *Bioinformatics (Oxford, England).* 2007;23(14):1846-7.

68. Jezequel P, et al. bc-GenExMiner: an easy-to-use online platform for gene prognostic analyses in breast cancer. *Breast cancer research and treatment.* 2012;131(3):765-75.

69. Ciriello G, et al. Comprehensive Molecular Portraits of Invasive Lobular Breast Cancer. *Cell.* 2015;163(2):506-19.

70. Pereira B, et al. The somatic mutation profiles of 2,433 breast cancers refines their genomic and transcriptomic landscapes. *Nature communications.* 2016;7:11479.

71. Gyorffy B, et al. An online survival analysis tool to rapidly assess the effect of 22,277 genes on breast cancer prognosis using microarray data of 1,809 patients. *Breast cancer research and treatment.* 2010;123(3):725-31.

72. Blacher S, et al. Cell invasion in the spheroid sprouting assay: a spatial organisation analysis adaptable to cell behaviour. *PloS one.* 2014;9(5):e97019.

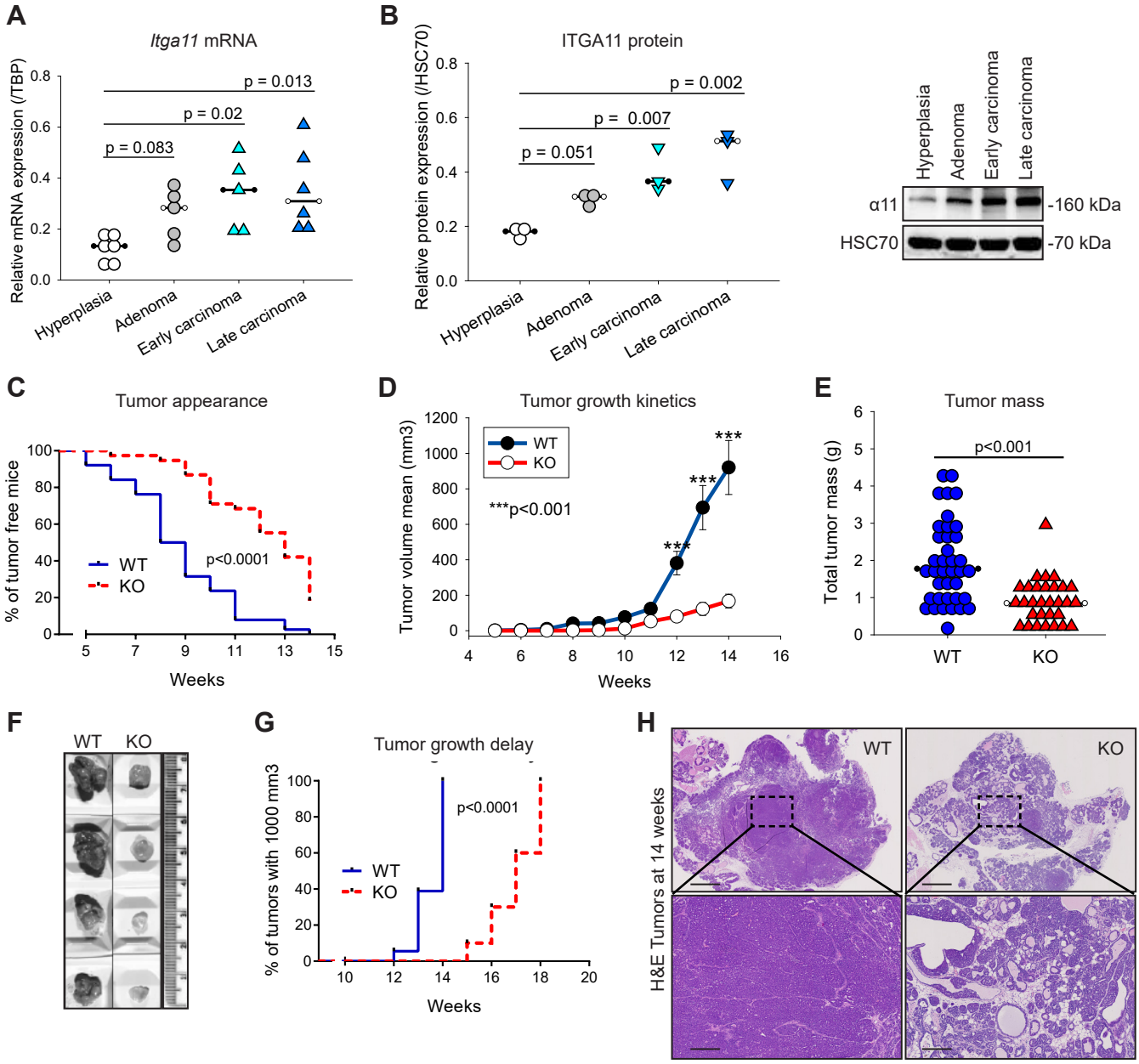

Figure 1. High integrin α11 expression associates with tumor progression in PyMT mouse breast tumor model. PyMT breast tumors analysed at different stages: hyperplasia, adenoma, early carcinoma and late carcinoma (5, 7, 10 and 14 weeks, respectively). (**A**) qRT-PCR of *Itga11* mRNA levels. Median of 5-6 tumors normalized to TBP. 1-way ANOVA with Holm-Sidak multiple comparison test. (**B**) Western blot of ITGA11 protein levels. Median of 3 tumors normalized to HSC-70. 1-way ANOVA with Holm-Sidak multiple comparison test. (**C**) Kaplan-Meier plot showing the appearance of palpable tumors in PyMT *Itga11*+/+ (WT) (n = 19) and *Itga11*-/- (KO) mice (n = 19). Log-rank (Mantel-Cox) test. (**D**) Tumor growth kinetics (n = 19 WT, n = 19 KO mice, 2 tumors/mouse). 2-Way ANOVA test with Holm-Sidak multiple comparison test. (**E**) Tumor mass at 14 weeks. Median of tumor mass (n = 38 WT; n = 30 KO tumors). Mann-Whitney test. (**F**) Representative pictures of tumors at sacrifice. (**G**) Kaplan-Meier plot showing tumor growth delay in KO mice. Data presented as the percentage of WT (n = 19) and KO (n = 29) mice reaching 1000 mm3 of tumor volume. Log-rank (Mantel-Cox) Test. (**H**) Representative images of haematoxylin & eosin staining of tumors. Bar scale: 2 mm (original); 0.5 mm (zoom).

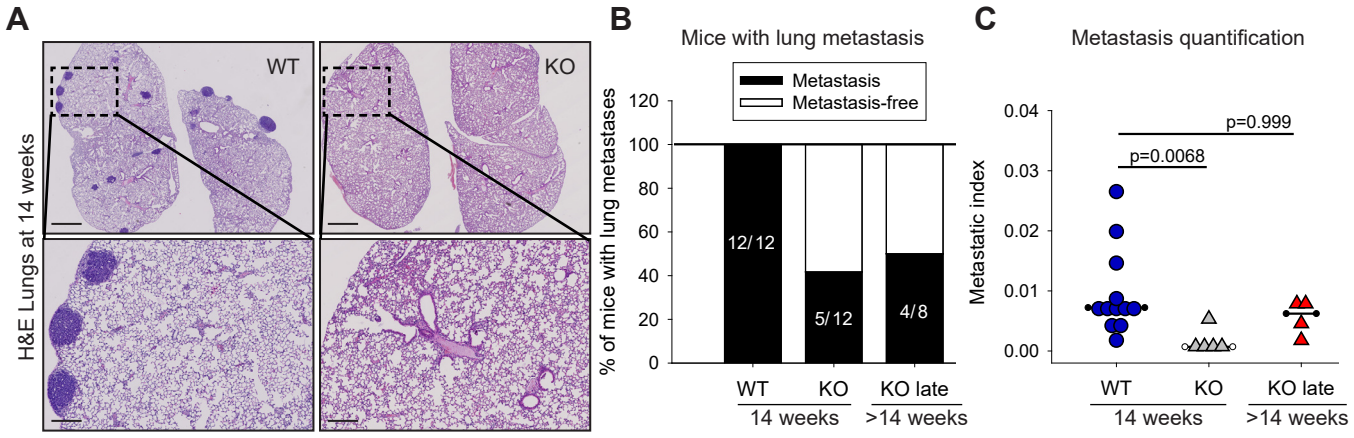

Figure 2. High integrin α11 expression associates with metastasis. (**A**) Representative images of haematoxylin & eosin staining of lungs issued from PyMT WT and KO mice. Bar scale: 1 mm (original); 250 µm (zoom). (**B-C**) Lung metastasis in mice at sacrifice (14 weeks for WT and KO groups and when tumors reached a 1000 mm3 volume for the "KO late" group). Results expressed as percentage of mice with lung metastasis (**B**) and median of metastatic index (lung tumor area/total lung area) analysed on mice bearing metastasis (**C**); n = 12 (WT); n = 5 (KO) n = 4 (KO late). 1-way ANOVA with Dunn's multiple comparison test.

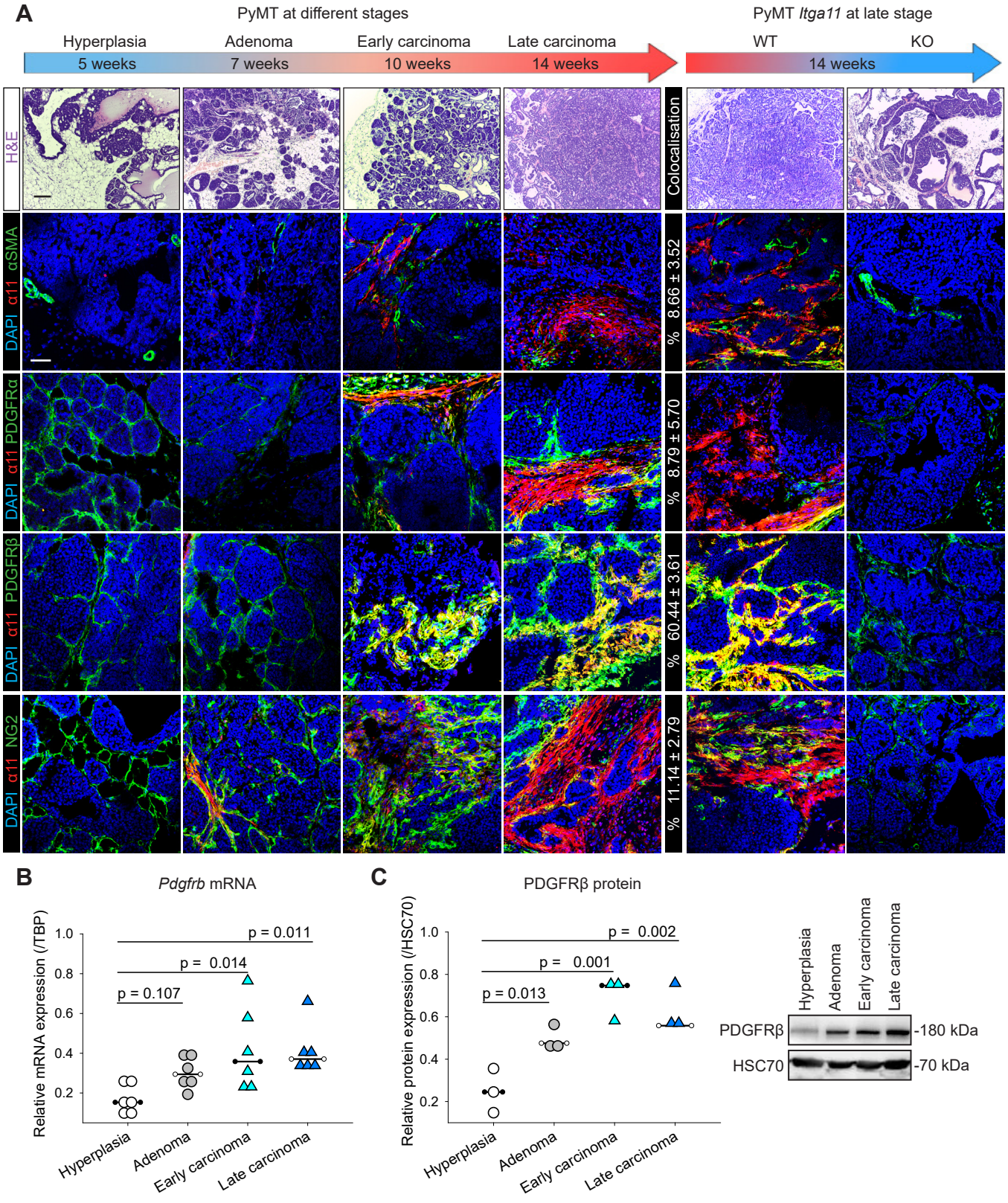

Figure 3. Integrin α11 defines a PDGFRβ+ CAF subpopulation and its expression is increased during tumor progression. (**A**) Representative pictures of haematoxylin & eosin and immunofluorescence staining of PyMT mice at different stages (left panel) and PyMT *Itga11* WT and KO mice at late stage (14 weeks) (right panel). Immunofluorescence confocal pictures show the co-staining of integrin α11 (red) and αSMA, PDGFRα or PDGFRβ (green). Nuclei stained with DAPI (blue). Scale bar: 50 µm. The % of cells positive for integrin α11 and a second marker compared to the total amount of α11+ cells are indicated ("colocalisation"). Colocalisation was determined by a computerized method on > 12 stromal fields/tumor (n = 8 for each genotype). (**B-C**) Quantification of *Pdgfrb* mRNA levels (qRT-PCR, data normalized to TBP) (n = 6) (**B**) and protein levels (Western blot, data normalized to HSC-70) (n = 3) (**C**) in PyMT tumors. Representative pictures of Western blots are shown in right panel. 1-way ANOVA with Holm-Sidak multiple comparison test.

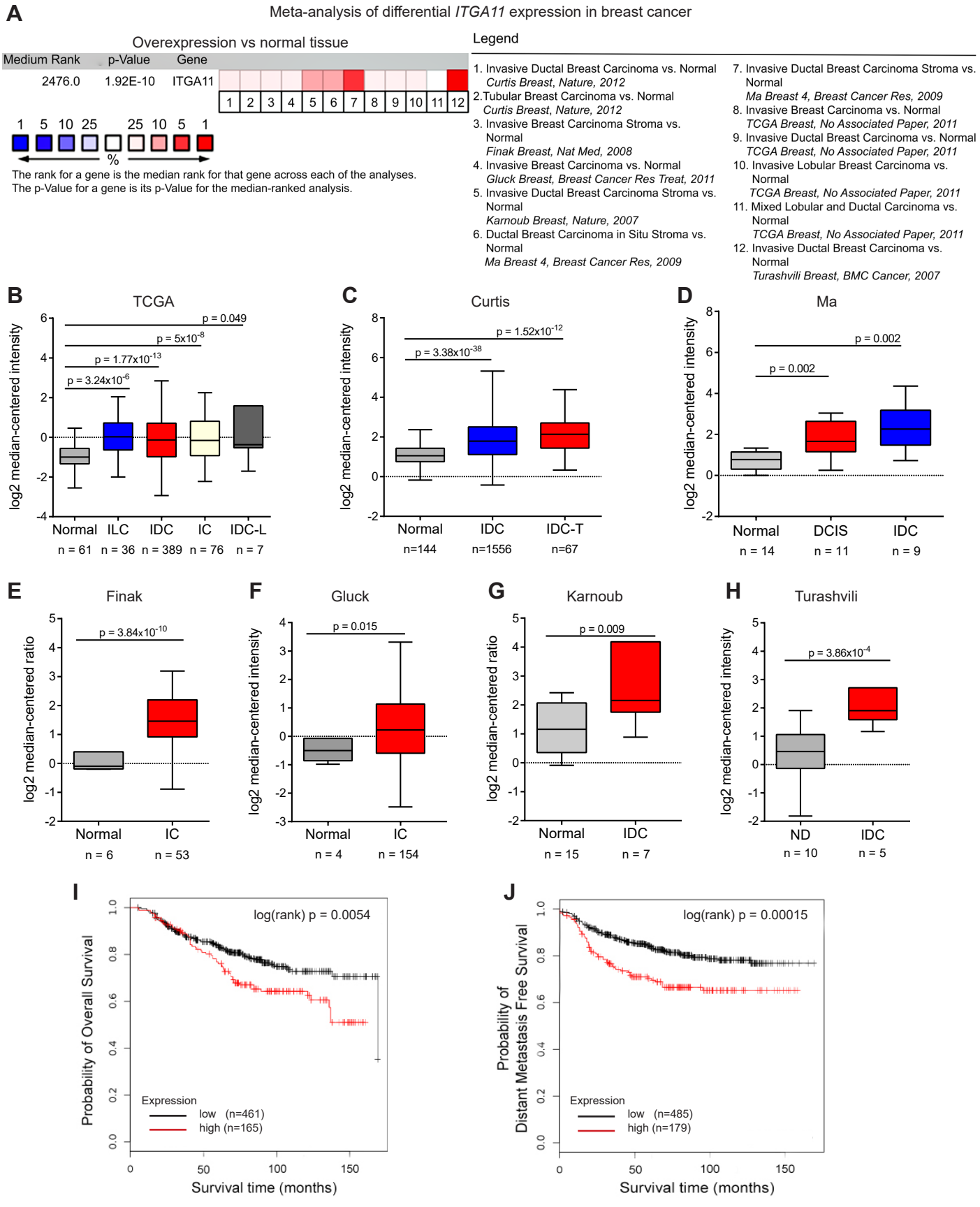

Figure 4. Integrin α11 expression is increased in human breast cancers. (**A**) Meta-analysis data of integrin α11 differential expression in breast cancers vs breast normal tissues. Oncomine microarray database was used to analyse *ITGA11* mRNA expression and meta-analysis was performed on 12 analyses from 7 microarray datasets (2375 patients). Data shown as median rank of *ITGA11* expression through each dataset analysis. *P*-value for *ITGA11* was determined by using the median ranked analysis of breast cancer vs. normal tissues. (**B-H**) Differential expressions of *ITGA11* mRNA in the 7 datasets included in the meta-analysis (Normal: normal adjacent breast tissue; IC: invasive breast carcinoma; IDC: invasive ductal breast carcinoma; IDC-L: mixed lobular and ductal breast carcinoma; IDC-T: invasive ductal breast carcinoma-tubular type; ILC: invasive lobular breast carcinoma). Median and interquartile range (10th and 90th percentiles). 2-sided *t*-test for two class differential expression analyses and Pearson's correlation for multiclass analyses. FDR-corrected *P*-values. (**I-J**) Kaplan-Meier plots showing the overall survival (**I**) and distant metastasis free survival (**J**) for *ITGA11* expression (probe: 23335_at). Log-rank *P*-values calculated in kmplot database.

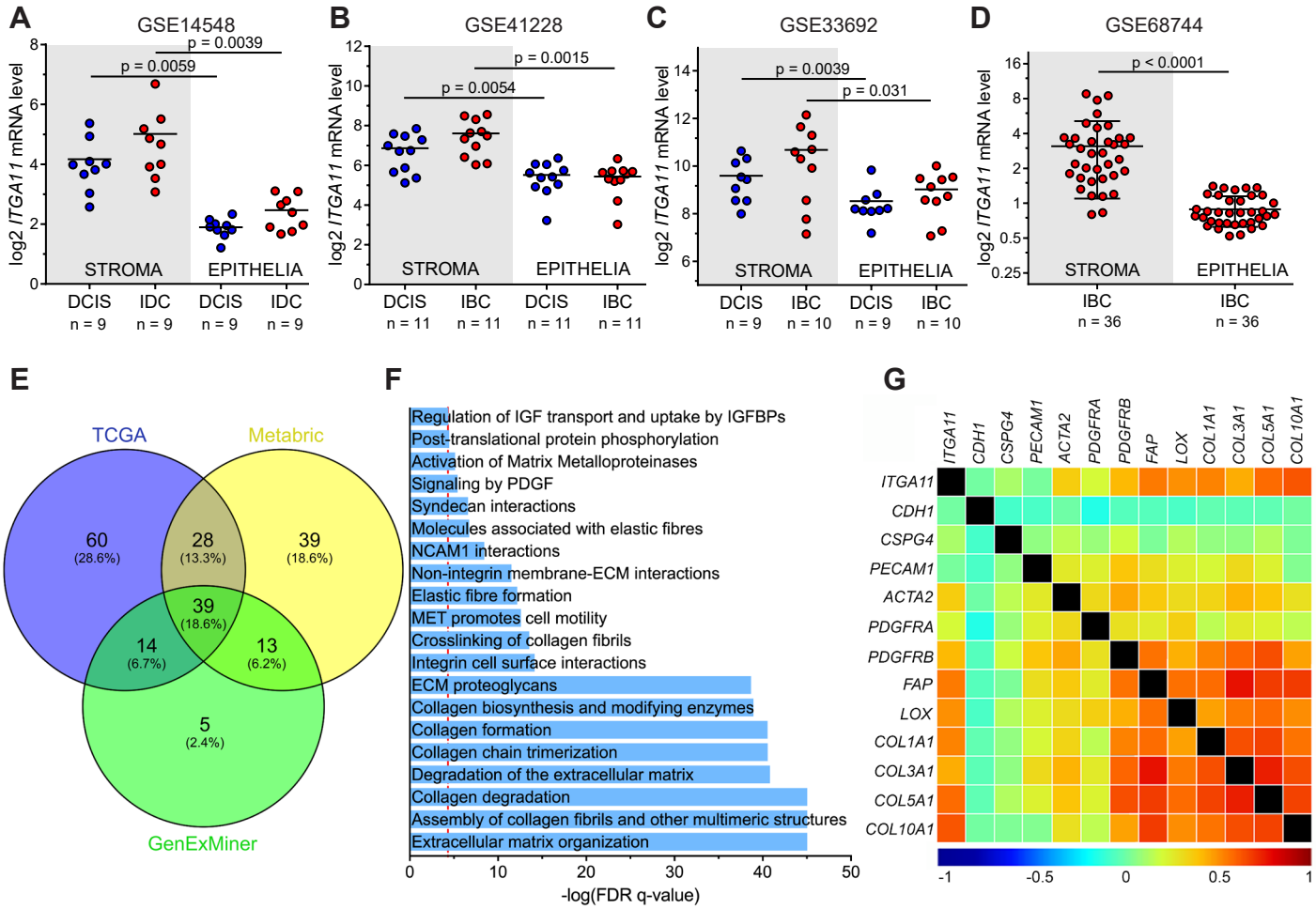

Figure 5. Integrin α11 expression correlates with a stromal gene signature in human breast cancer. (**A-D**) *ITGA11* mRNA expression in microdissected stromal and epithelial compartments from ductal carcinoma in situ (DCIS) and invasive ductal (IDC)/invasive breast (IBC) carcinoma issued from GSE14548 (**A**), GSE41228 (**B**), GSE33692 (**C**) and GSE68744 (**D**) datasets. The $\log_2$ transformed *ITGA11* expression values were exported from GEO2R and analysed in GraphPad Prism. Significance assessed by paired 2-tailed *t*-test (normal distribution) and Wilcoxon matched-pairs signed rank test (non-normal distribution). (**E**) Venn diagrams depicting the overlap and number of genes associated with *ITGA11* expression in BC across 3 genomic datasets (TCGA, Metabric and GenExMiner). (**F**) Reactome pathway-enriched analysis showing biological processes and pathways correlated with *ITGA11*-associated gene signature (top 20 significant pathways). Red dotted line, FDR-adjusted *Q*-value = 0.05. (**G**) Targeted heat matrix showing correlation between *ITGA11* and twelve selected genes representing different tumor-associated cell populations. Data mining was performed by using bc-GenExMiner 4.1. Colour scale depicts Pearson's correlation coefficients from -1 (dark blue, strong negative correlation) to +1 (dark red, strong positive correlation).

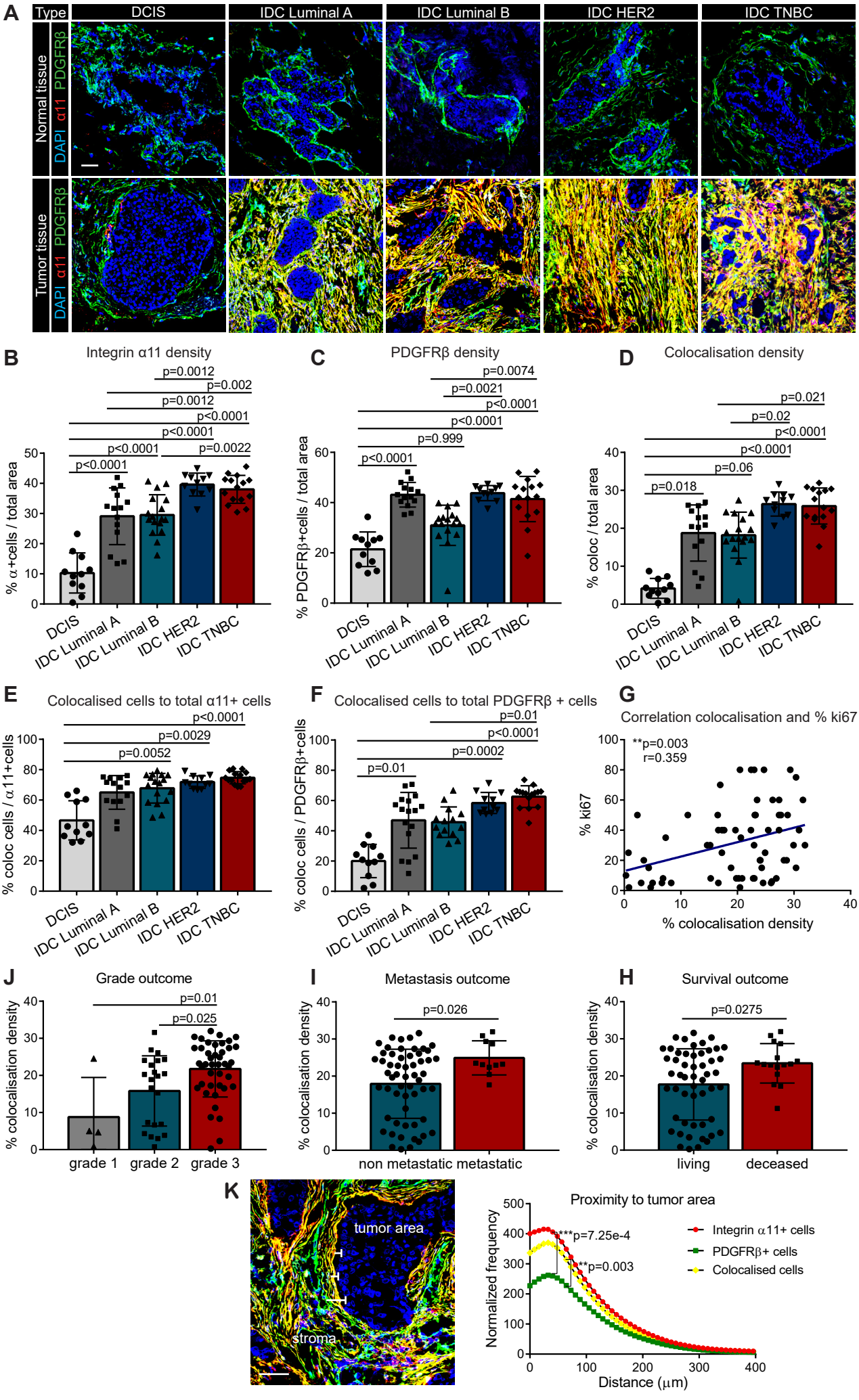
A
Type
DCIS
IDC Luminal A
IDC Luminal B
IDC HER2
IDC TNBC
Normal tissue
DAPI α11 PDGFRβ
Tumor tissue
DAPI α11 PDGFRβ
B
Integrin α11 density
% α+cells / total area
p=0.0012
p=0.002
p=0.0012
p<0.0001
p<0.0001
p<0.0001
p=0.0022
p<0.0001
C
PDGFRβ density
% PDGFRβ+cells / total area
p=0.0074
p=0.0021
p<0.0001
p<0.0001
p=0.999
p<0.0001
D
Colocalisation density
% coloc / total area
p=0.021
p=0.02
p<0.0001
p<0.0001
p=0.06
p=0.018
DCIS
IDC Luminal A
IDC Luminal B
IDC HER2
IDC TNBC
E
Colocalised cells to total α11+ cells
% coloc cells / α11+cells
p<0.0001
p=0.0029
p=0.0052
F
Colocalised cells to total PDGFRβ + cells
% coloc cells / PDGFRβ+cells
p=0.01
p<0.0001
p=0.0002
p=0.01
G
Correlation colocalisation and % ki67
**p=0.003
r=0.359
% ki67
% colocalisation density
J
Grade outcome
% colocalisation density
p=0.01
p=0.025
grade 1
grade 2
grade 3
I
Metastasis outcome
% colocalisation density
p=0.026
non metastatic
metastatic
H
Survival outcome
% colocalisation density
p=0.0275
living
deceased
K
tumor area
stroma
Proximity to tumor area
Normalized frequency
***p=7.25e-4
**p=0.003
Integrin α11+ cells
PDGFRβ+ cells
Colocalised cells
Distance (μm)

Figure 6. Integrin α11/PDGFRβ density is associated with a poor clinical outcome in breast cancer. (**A**) Representative confocal pictures of immunofluorescence co-staining of integrin α11 (red) and PDGFRβ (green) in human breast samples: tumor tissues and normal associated tissues from patients with ductal carcinoma in situ (DCIS) and invasive (IDC) of luminal A and B, HER2 or triple negative breast cancers (TNBC). Scale bar: 50 µm. Nuclei stained with DAPI (blue). (**B-D**) Quantification of integrin α11 (**B**), PDGFRβ (**C**) and their colocalisation (**D**) density on BC samples. Data presented as % of stained area normalized to total tumor area. n = 68 patients (n = 11 DCIS, n = 14 IDC Luminal A, n = 17 IDC Luminal B, n = 11 IDC HER2, n = 15 IDC TNBC). 1-way ANOVA with Dunnett's (**B**) and Kruskal-Wallis with Dunn's multiple comparison tests (**C-D**). (**E-F**) Overall % of integrin α11/PDGFRβ+ cells normalised to total integrin α11+ (**E**) or PDGFRβ+ cells (**F**). Minimum 6 stromal fields/ tumor, n = 68 patients. Kruskal-Wallis with Dunn's multiple comparison test. (**G**) Correlation of integrin α11/PDGFRβ colocalisation density from (**D**) with % of ki67 in human BC. n = 68 patients. Pearson correlation analysis. (**J-H**) Association of integrin α11/PDGFRβ colocalisation density with BC grade (**J**), metastasis (**I**) and survival (**H**) outcomes. n = 68 patients. 1-way ANOVA with Tukey's multiple comparison (**J**) and Mann-Whitney (**I-H**) tests. (**K**) Quantification of spatial enrichment of integrin α11 (red), PDGFRβ (green) and colocalisation (yellow) areas vs tumor areas in human BC samples. Data presented as frequency of stained pixels as a function of the distance to tumor areas. n = 56 stromal fields. Significance between the distribution curves determined by Kolmogorov-Smirnov test within the distance range of 0-100 µm.

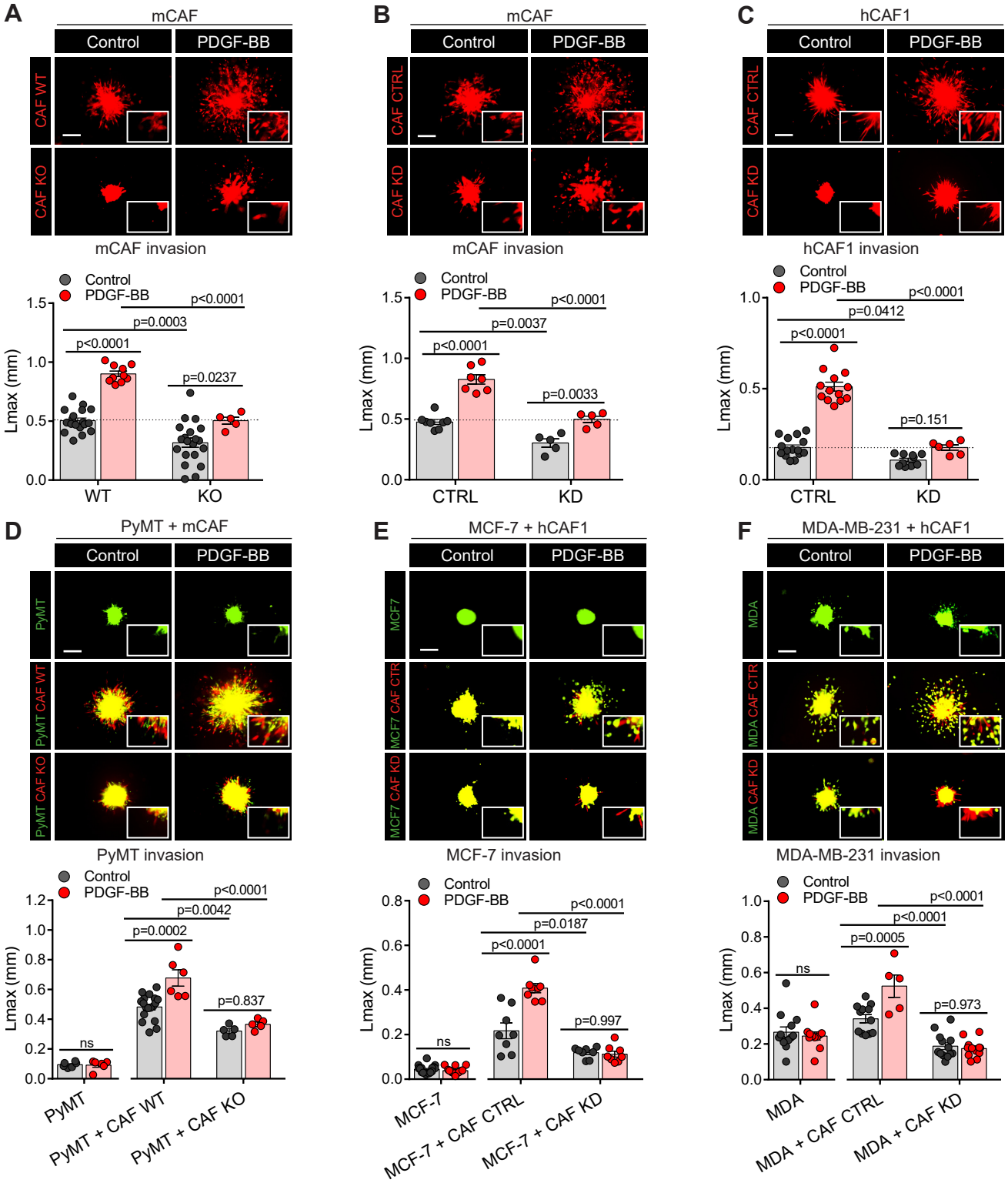

Figure 7. Integrin α11-expressing CAFs promote *in vitro* tumor cell invasion in response to PDGF-BB. (**A-C**) Representative spheroid pictures of red-tracked mCAFs WT and KO (**A**), mCAFs CTRL and KD (**B**), hCAF1 CTRL and KD (**C**) after 20 h of invasion in a 3D collagen matrix stimulated with PDGF-BB (10 ng/ml). Scale bar: 200 µm. Zoomed pictures (2X) in right lower panels. Cell invasion quantification presented in lower panels. Data expressed as maximal distance of invasion from the spheroid border (Lmax). n = 5-20 (**A**); n = 5-8 (**B**); n = 6-15 (**C**). Representative of 3 independent experiments. 1-way ANOVA with Tukey's multiple comparison test. (**D-F**) Representative homo- and heterospheroid pictures of green-tracked PyMT tumor cells and red-tracked mCAFs WT and KO (**D**) and green-tracked MCF-7 and MDA-MB-231 tumor cells and red-tracked hCAF1 CTRL and KD (**E-F**) after 20 h of seeding in collagen. Scale bar: 200 µm. Zoomed pictures (2X) in right lower panels. Lower panels correspond to tumor cell invasion quantification (Lmax). n = 5-18 (**D**); n = 8-19 (**E**); n = 5-13 (**F**). Representative of 3 independent experiments. 1-way ANOVA with Tukey's multiple comparison test.

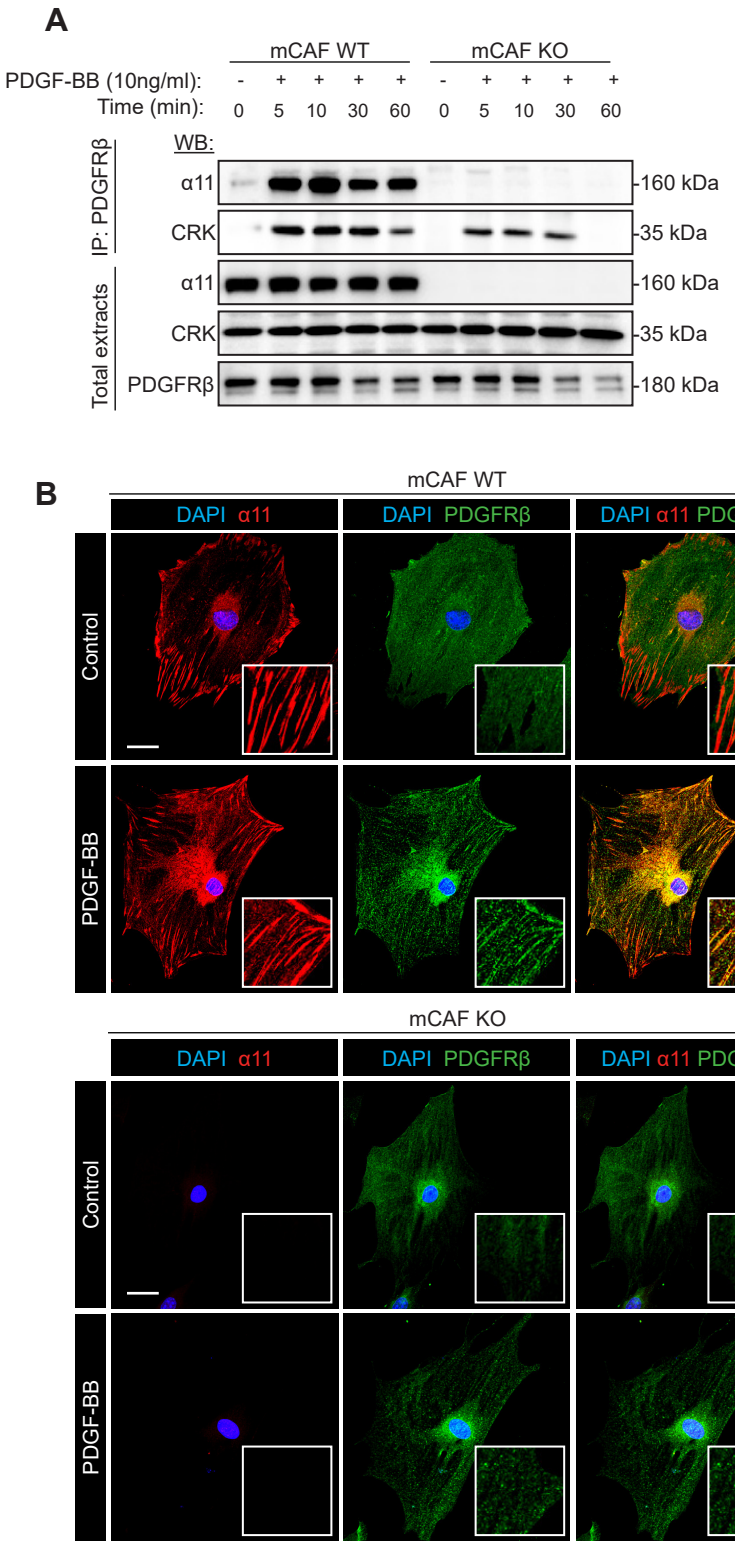

Figure 8. Integrin α11 interacts with PDGFRβ in a ligand-dependent manner. (**A**) Western blot kinetics of PDGFRβ co-immunoprecipitation with integrin α11 and CRK in response to PDGF-BB (10 ng/ml) after 0, 5, 10, 30 and 60 min of treatment in mCAFs WT and KO. Total extracts are shown in the corresponding lower panels. (**B**) Confocal immunofluorescence colocalisation of integrin α11 (red) and PDGFRβ (green) before (Control) and after treatment with PDGF-BB (10 ng/ml) for 10 min in mCAFs WT and KO. Nuclei counterstained with DAPI. Scale bar: 40 μm.

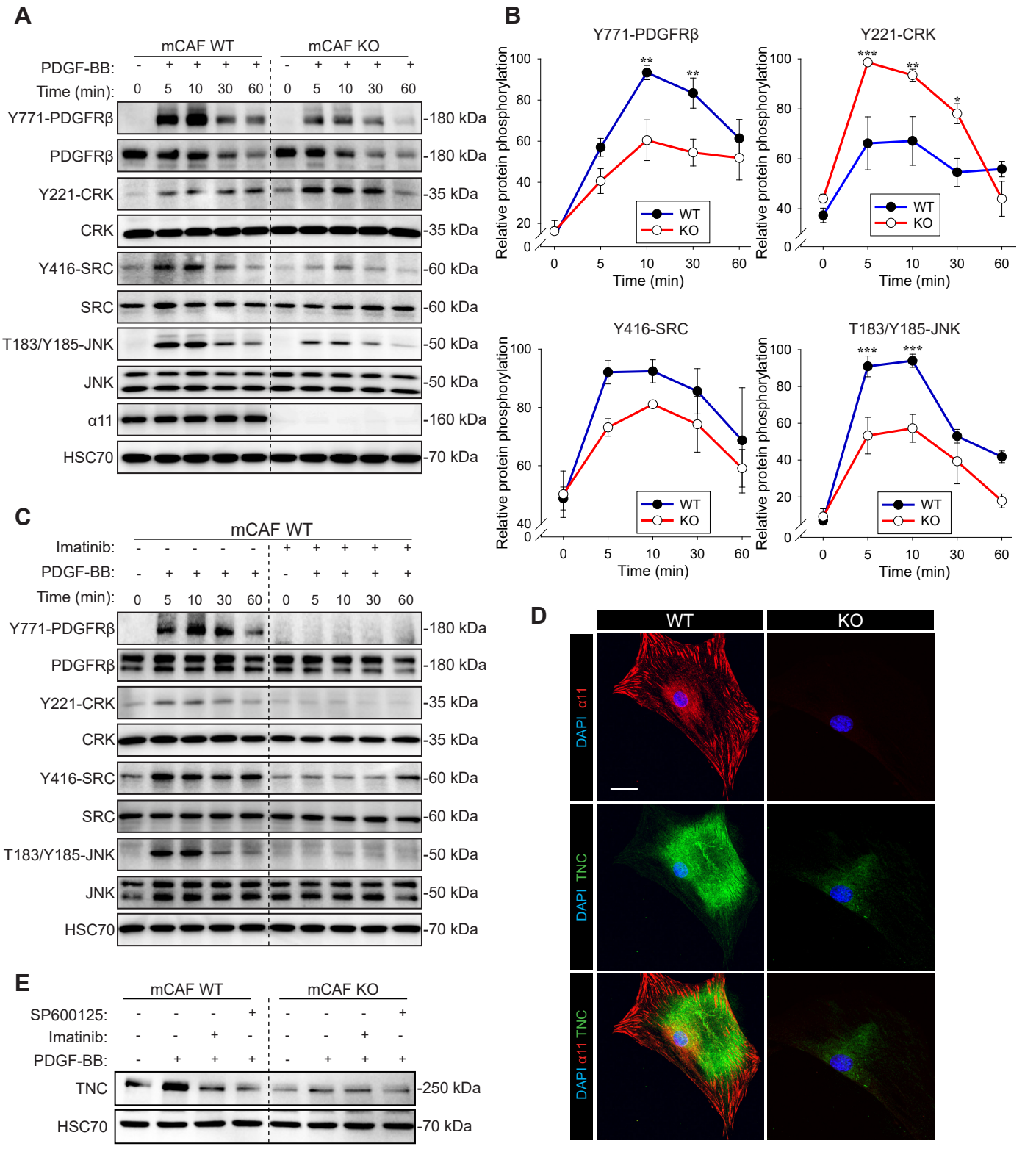

Figure 9. Integrin α11 regulates PDGFRβ downstream activation and promotes Tenascin C expression in CAFs. (**A**) Western blot of protein phosphorylation for PDGFRβ (Y771), CRK (Y221), SRC (Y416) and JNK (T183/S185) after 0, 5, 10, 30 and 60 min of PDGF-BB (10 ng/ml) stimulation in mCAFs WT and KO. (**B**) Quantified kinetics of PDGFRβ, CRK, SRC, JNK protein phosphorylation from (**A**). Data presented as normalized ratio between phosphorylated and total proteins. n = 7 (Y771-PDGFRβ); n = 4 (Y221-CRK); n = 3 (Y416-SRC) and n = 4 (T183/Y185-JNK) of independent experiments. 2-way ANOVA with Holm-Sidak multiple comparison test. (**C**) Western blot of protein phosphorylation for PDGFRβ (Y771), CRK (Y221), SRC (Y416) and JNK (T183/S185) after PDGF-BB (10 ng/ml) stimulation in mCAFs WT pre-treated or not with Imatinib (5 μM) for 1.5 h. (**D**) Confocal immunofluorescence staining of integrin α11 (red) and Tenascin C (TNC) (green) in mCAFs WT and KO. Nuclei stained with DAPI. Scale bar: 40 μm. (**E**) Western blot analysis of Tenascin C expression before or after PDGF-BB (10 ng/ml) stimulation in mCAFs WT and KO pre-treated or not with Imatinib (5 μM) or SP600125 (5 μM) for 20 h.

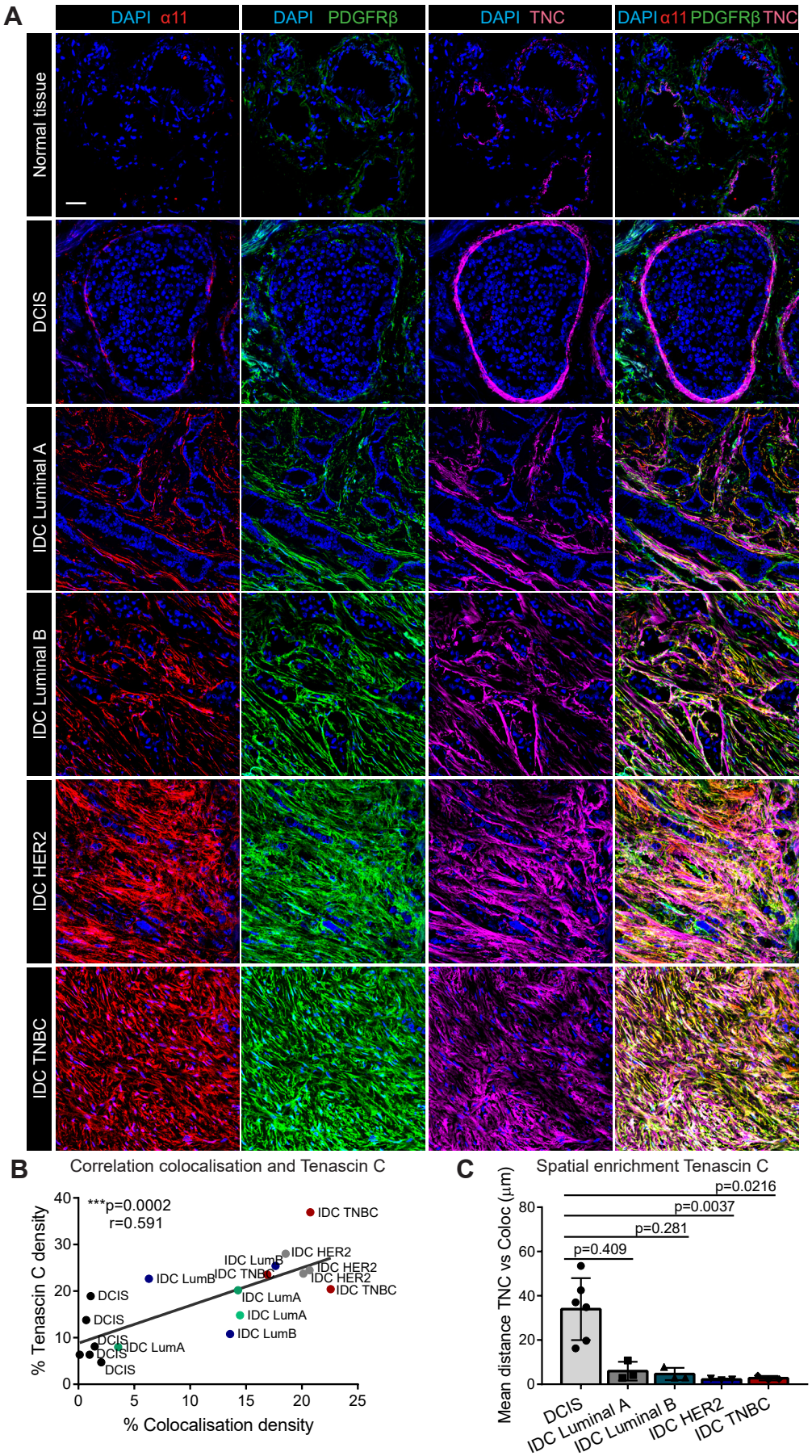

Figure 10. Integrin α11/PDGFRβ density is associated with a Tenascin C enrichment in human breast cancer. (**A**) Representative immunofluorescence pictures of integrin α11 (red), PDGFRβ (green) and Tenascin C (TNC) (pink) co-staining in human breast samples: normal associated breast tissue, ductal carcinoma in situ (DCIS) and invasive ductal carcinomas (IDC) from luminal A and B, HER2 or TNBC patients. Scale bar: 50 µm. Nuclei stained with DAPI. (**B**) Correlation of integrin α11/PDGFRβ colocalisation density with TNC expression on human breast cancer samples from (**A**). Data presented as percentage of density (stained area/total tumor area). n = 18 patients (n = 6 DCIS, n = 3 IDC Luminal A, n = 3 IDC Luminal B, n = 3 IDC HER2, n = 3 IDC TNBC). Pearson correlation analysis. (**C**) Spatial enrichment of TNC versus integrin α11/PDGFRβ colocalised areas in BC samples from (**A-B**). Data presented as mean of the euclidean distance of TNC to colocalised areas. n = 18 patients. Kruskal-Wallis with Dunn's multiple comparison test.

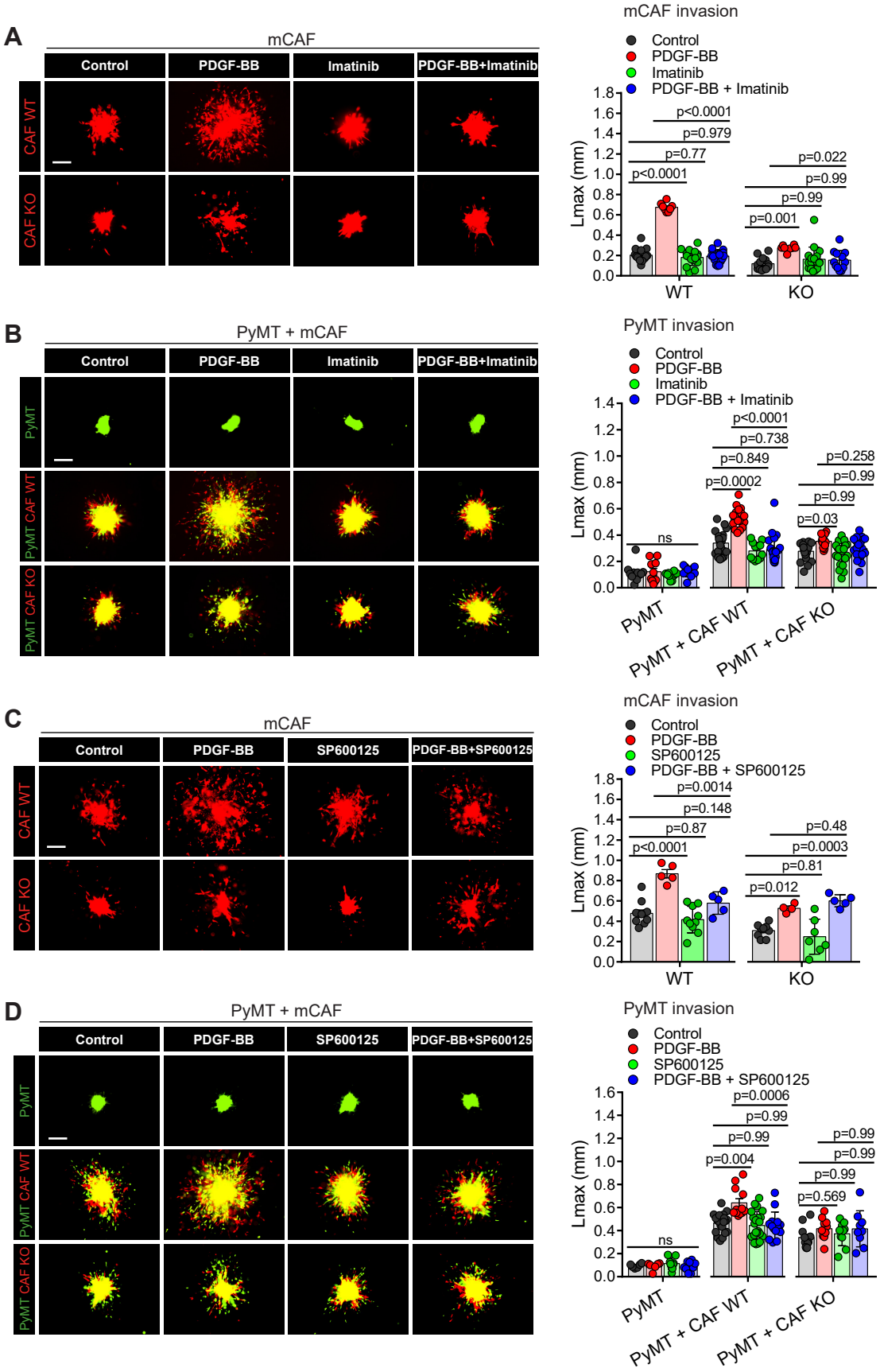

Figure 11. Pharmacological inhibition of PDGFRβ or JNK reverses PDGF-BB-induced invasiveness of integrin α11 WT CAFs and of cancer cells in heterospheroids. (**A, C**) Representative homospheroid pictures of red-tracked mCAFs WT and KO after 20 h of invasion in collagen in response to PDGF-BB (10 ng/ml) and upon treatment with 5 μM of Imatinib (PDGFRβ inhibition) (**A**) or SP600125 (JNK inhibition) (**C**). Scale bar: 200 μm. Quantification of cell invasion presented in the corresponding graphs. Data expressed as maximal distance of invasion from the spheroid border (Lmax). n = 8-17 (**A**); n = 5-11 (**C**). Kruskal-Wallis with Dunn's multiple comparison (**A**) and 1-way ANOVA with Tukey's multiple comparison (**C**) tests. (**B, D**) Representative homo- and heterospheroid pictures of green-tracked PyMT tumor cells and red-tracked mCAFs WT and KO after 20 h of invasion in response to PDGF-BB (10 ng/ml) and upon treatment with 5 μM of Imatinib (**B**) or SP600125 (**D**). Scale bar: 200 μm. Quantification of tumor cell invasion (Lmax) presented in the corresponding graphs. n = 12-21 (**B**); n = 9-22 (**D**). Kruskal-Wallis with Dunn's multiple comparison test.